Phase equilibria modelling constraints on *P–T* conditions during fluid catalysed conversion of granulite to eclogite in the Bergen Arcs, Norway

K. Bhowany[1], M. Hand[1], C. Clark[2], D. E. Kelsey[1], S. M. Reddy[2], M. A. Pearce[3], N. M. Tucker[1], L. J. Morrissey[4]

1. *Department of Earth Sciences, School of Physical Sciences, University of Adelaide, Adelaide, SA 5000, Australia.*
2. *Department of Applied Geology , Core to Crust Fluid Systems ARC COE, Curtin University, Perth, WA 6102, Australia.*
3. *CSIRO Mineral Resources, Australian Resources Research Centre, Perth, WA 6151, Australia*
4. *School of National and Built Environments, University of South Australia, Adelaide, Australia*

Corresponding author:
kamini.bhowany@adelaide.edu.au

ABSTRACT

Exhumed eclogitic crust is rare and exposures that preserve both protoliths and altered domains are limited around the world. Nominally anhydrous Neoproterozoic anorthositic granulites exposed on the island of Holsnøy, in the Bergen Arcs in western Norway, preserve different stages of progressive prograde deformation, together with the corresponding fluid-assisted metamorphism, which record the conversion to eclogites during subduction associated with the Ordovician-Silurian Caledonian Orogeny. Four different stages of deformation can be identified: 1) brittle deformation resulting in the formation of fractures and the generation of pseudotachylites in the granulite; 2) development of mesoscale shear zones associated with increased fluid–rock interaction; 3) the complete large-scale replacement of granulite by hydrous eclogite with blocks of granulite sitting in an eclogitic 'matrix'; and 4) the break-up of completely eclogitised granulite by continued fluid influx, resulting in the formation of coarse-grained phengite-dominated mineral assemblages. *P–T* constraints derived from phase equilibria forward modelling of mineral assemblages associated with some stages of the deformation evolution document a burial and partial exhumation path with peak metamorphic conditions occurring at 21–22 kbar and 670–690 °C. The *P–T* models, in combination with existing *T–t* constraints, imply that the Lindås Nappe underwent extremely rapid retrogressive pressure change. Fluid infiltration began on the prograde burial path and continued throughout the recorded *P–T* evolution, implying a fluid source that underwent progressive dehydration during subduction of the granulites. However, in places limited fluid availability on the prograde path resulted in assemblages largely consuming the available fluid, essentially freezing in snapshots of the prograde evolution. These were carried metastably deeper into the mantle with strain partitioned into areas where ongoing fluid infiltration was concentrated.

Key words: Bergen Arcs, Holsnøy, eclogite, *P–T* conditions, fluid-infiltration

INTRODUCTION

A number of studies have explored the way in which fluids can be generated during prograde dehydration accompanying subduction (e.g. Peacock, 1990; Peacock, 1993; Liu *et al.*, 1996; Schmidt & Poli, 1998; Spandler *et al.*, 2003; Groppo & Castelli, 2010). Using calculated mineral modal proportions and compositions, Hacker *et al.* (2003) demonstrated that subducted (and exhumed) lithologies generally retain less water than their less buried equivalents. It follows that for the most part, the record of fluid expulsion is an inverse one, where the formation of comparatively anhydrous co-product assemblages are the record of fluid generation and loss (Guiraud *et al.*, 2001; Baxter & Caddick, 2013). For example, Dragovic *et al.* (2012) and Baxter and Caddick (2013) showed that the formation of garnet-bearing assemblages during subduction could be used to make estimates of the amount fluid released during increasing temperature, and demonstrated that rates of fluid generation are not steady state, but rather are punctuated around prograde mineral reactions. More generally, similar models have been formulated for fluid release during prograde metamorphic dehydration in non-subduction settings (e.g. Philippot, 1993; Stüwe, 1998; Vry *et al.*, 2010). A consequence of punctuated fluid generation is that fluid flow events in subducting systems are probably also punctuated, resulting in comparatively short-lived fluid–rock interactions.

While recrystallization and dehydration of subducted fluid-bearing rocks leads to predictable mineral assemblages and fluid generation, the fate of subducted nominally anhydrous rocks such as continental granulites is less predictable. From an equilibrium thermodynamic standpoint, the conversion of granulite across a wide range of compositions to compositionally equivalent eclogite should occur in response to changes in pressure and temperature (Ridley, 1984; Lardeaux & Spalla, 1991; Ghent *et al.*, 2004). However, a few

studies have shown that anhydrous granulitic rocks are usually stable, and hence their conversion to eclogite is not kinetically favourable, with the result that large tracts of dry granulitic crust can be transported into the mantle and return to the surface with little mineralogical modification (e.g. Ellis & Maboko, 1992; Austrheim *et al.*, 1997; Jackson *et al.*, 2004). On the other hand, the conversion of dry granulite to eclogite can be catalysed by interaction with fluids (e.g. Austrheim & Griffin, 1985; Erambert & Austrheim, 1993; Jolivet *et al.*, 2005; Terry & Heidelbach, 2006; Martin *et al.*, 2011). Such catalysis leads to the development of hydrous mineral assemblages that may result in changes in the rheology and bulk density of the deeply buried crust (e.g. Erambert & Austrheim, 1993; Rockow *et al.*, 1997; Engvik *et al.*, 2000; Pollok *et al.*, 2008; Connolly, 2009). While the generation of fluids in hydrous subducted rocks will leave a dehydrated mineralogical record, anhydrous granulites can potentially record fluid release events via the formation of hydrous mineralogies that mark the absorption of fluid released elsewhere by dehydration. Given the importance of fluid in catalysing reactions in previously anhydrous rocks, the product mineral assemblages are likely to be frozen in when the fluid pulse is exhausted, or consumed by the product assemblages. These hydrous mineral assemblages therefore have the potential to record the Pressure–Temperature (*P–T)* conditions at which fluid was able to migrate from a dehydrating source region(s) during the subduction and exhumation of granulitic crust.

In the Lindås Nappe in the Bergen Arcs, western Norway, white mica- and epidote-group-bearing (i.e. hydrous) high-*P* amphibolite and eclogite occur extensively within granulitic protolith (Fig. 1). The granulites are early Neoproterozoic in age (c. 950 Ma) whereas the eclogites are Ordovician-aged (c. 450 Ma; Van Wyck *et al.*, 1996; Bingen *et al.*, 2001; Bingen *et al.*, 2004; Austrheim, 2013). The formation of the high-*P* mineral assemblages is interpreted to have occurred during H_2O-rich fluid infiltration—a form of deep crustal

metasomatism—along fractures and shear zones during the Caledonian Orogeny (Austrheim & Griffin, 1985; Andersen *et al.*, 1990; Boundy *et al.*, 1992; Austrheim, 2013). Mineralogically and geochemically, the evidence for fluid infiltration is confirmed by the presence of potassium-rich mica, epidote-group minerals and the presence of quartz veins within the host plagioclase–clinopyroxene–orthopyroxene–garnet anorthositic granulite (Austrheim & Griffin, 1985; Andersen *et al.*, 1990; Andersen *et al.*, 1991c; Boundy *et al.*, 1992; Raimbourg *et al.*, 2005; Austrheim, 2013).

Numerous studies have investigated the development of the fluid–rock system in the Lindås Nappe (e.g. Austrheim & Griffin, 1985; Andersen *et al.*, 1991c; Bingen *et al.*, 2001; Raimbourg *et al.*, 2005; Russell *et al.*, 2012; Austrheim, 2013). However, there are comparatively few robust constraints on the *P–T* conditions at which fluid–rock interaction occurred. Existing constraints of 15–21 kbar and 650–800 °C were derived from conventional thermobarometry (Fe–Mg exchange between garnet and omphacite and garnet and amphibole; Austrheim & Griffin, 1985; Jamtveit *et al.*, 1990; Boundy *et al.*, 1996; Boundy *et al.*, 1997). More recently, Raimbourg *et al.* (2007) used the Gibbs energy minimisation methods to derive rudimentary phase diagrams in concert with average *P–T* calculations (Powell & Holland, 1988; Holland & Powell, 1990; Holland & Powell, 1998) to derive *P–T* conditions of 20 kbar and 720 °C. However, there is little of a systematic *P–T* information for the different stages of fluid–rock interaction recorded in the Lindås Nappe, particularly the stages that lead to the development of the eclogitic assemblages. Better constrained *P–T* information will provide a framework in which to understand the origins of the metasomatising fluids. In this study, field structural relationships on the island of Holsnøy were used to identify different stages of deformation and recrystallization in the modification of the granulite protolith to eclogite. Samples from these different stages were then used in

phase equilibria forward modelling to constrain the framework for the evolving *P–T* conditions under which eclogitisation occurred.

GEOLOGICAL SETTING

Study area

Holsnøy is located in south-western Norway, approximately 45 km north-west of Bergen. The outcropping rocks on Holsnøy form part of the Lindås Nappe, which is one of the major domains of the Bergen Arcs (Austrheim, 2013; Centrella *et al.*, 2015). It is arguably one of the best locations in the world to study deep crustal metasomatism, as both the protolith (granulite) and metasomatic product (eclogite) are superbly preserved, and a number of studies have documented the fluid–rock interactions in this area (e.g. Mattey *et al.*, 1994; Jolivet *et al.*, 2005; Raimbourg *et al.*, 2005; Austrheim, 2013; Centrella *et al.*, 2015). This study focuses on north-eastern Holsnøy (Fig.1), where the main eclogitised granulite can be found along with different deformational features associated with the transformation of granulite to eclogite.

Structural features and stages of deformation

The granulite facies, anorthositic protolith was metamorphosed at approximately 950 Ma (Krogh, 1977; Austrheim & Griffin, 1985; Pollok *et al.*, 2008) during the Grenvillian-aged Sveconorwegian Orogeny (Austrheim & Griffin, 1985; Austrheim, 1987). The granulite is dominated by plagioclase with lesser clinopyroxene, garnet and orthopyroxene. Garnet and clinopyroxene commonly form coronae around orthopyroxene, and are aligned with the foliation of the granulite (Raimbourg *et al.*, 2005; Austrheim, 2013). *P–T* estimates from

conventional thermobarometry for the granulite facies peak metamorphic conditions are 10 kbar and 800–900 °C (Austrheim, 1987; Boundy *et al.*, 1997; Austrheim, 2013).

The anorthositic granulites were subsequently deeply buried during the Caledonian Orogeny at c. 450 Ma and partially to completely converted to high-*P* amphibolite and eclogite (Austrheim & Griffin, 1985; Boundy *et al.*, 1996; Van Wyck *et al.*, 1996; Glodny *et al.*, 2008). There has been less focus on the high-*P* amphibolite facies assemblages that preceded the eclogite assemblage. However, petrology of the eclogite has been previously described in detail (Austrheim & Griffin, 1985; Jamtveit *et al.*, 1990; Boundy *et al.*, 1992; Austrheim *et al.*, 1997; Bingen *et al.*, 2001; Raimbourg *et al.*, 2005; Pollok *et al.*, 2008). The essential mineralogy of the eclogites consists of garnet, omphacite and zoisite. Depending on rock composition, the eclogites may also contain varying amounts of phengite, kyanite, rutile and quartz as well as retrograde amphibole. Previous *P–T* constraints for their formation (15–21 kbar and 650–800 °C) suggest burial depths of approximately 50–70 km (Austrheim, 1987; Jamtveit *et al.*, 1990; Boundy *et al.*, 1996; Boundy *et al.*, 1997; Pollok *et al.*, 2008; Austrheim, 2013). Later reworking of the eclogite is interpreted to be associated with partial exhumation at amphibolite facies conditions to have occurred at lower *P–T* conditions of 8–12 kbar and 600–700 °C (Kühn, 2002; Glodny *et al.*, 2008). The transition from granulite to eclogite on Holsnøy has been described by a number of workers (Austrheim, 1987; Jamtveit *et al.*, 1990; Boundy *et al.*, 1992; Boundy *et al.*, 1997; Kühn *et al.*, 2002; Jolivet *et al.*, 2005; Raimbourg *et al.*, 2007), and can be seen via different stages of deformation that progressively increase the degree of transformation of the protolith.

Stage 1 involves the formation of pseudotachylite arrays and veins. These have been described in detail by Austrheim and Boundy (1994), Austrheim *et al.* (1996) and Austrheim

et al. (2017). The pseudotachylites now occur in the granulites as recrystallised pale grey veins and injection structures. They either cross-cut the granulite foliation (Fig. 2a) or follow its trend (Fig. 3a). Where the veins follow the foliation, they form thin (2–4 cm) dyke like structures that can be traced continuously for up to 20 m. These dyke-like veins have irregularly shaped injection veins that transect the enclosing granulitic foliation. In other instances the pseudotachylites form arrays within foliation-discordant domains up to 1 m wide (Fig. 3a), within which numerous irregular centimetre-scale pseudotachylite veins occur. In places rotation and disruption of the granulite foliation has occurred, creating crushed zones that also contain cataclasites and ultramylonites (Austrheim & Boundy, 1994; Austrheim *et al.*, 1996). The pseudotachylites have been overprinted by high-*P* amphibolite and eclogite assemblages that formed during fluid infiltration. The formation of the pseudotachylites is probably linked to the Caledonian Orogeny due to their consistent proximity to eclogitised shear zones (Austrheim & Boundy, 1994).

Stage 2 involved the formation of discrete shear zones that range from centimetre- to metre-scale within metasomatised granulite (Fig. 2b). The metasomatism is marked by a darkening of the granulite to form grey–green regions with a diffuse and gradational transition to the granulite (Fig. 2b). These regions of alteration and associated plastic deformation overprint the stage 1 pseudotachylite (Fig. 3a). The alteration comprises polygonal recrystallised plagioclase grains, together with zoisite, kyanite, omphacite and phengite. Garnet grains inherited from the granulite protolith have been partially consumed, with modal reductions of ~ 50% compared to the granulite protolith, and form relict grains in the alteration assemblage. The domains of altered granulite typically follow the shear zones and contain structurally reworked granulite (Fig. 3b). However, in some instances the granulite is altered without any associated deformation, with the existing foliation passing smoothly through the region of

alteration. Where stage 2 deformation and alteration are volumetrically minor, the pre–existing granulite facies structures can be traced continuously through the outcrops and are only modified where they are deflected into discrete shear zones (Fig. 3b).

Stage 3 involved a significant increase in alteration of the granulite within shear zones that are tens of metres in width and kilometres in length. The metasomatised rock is the complete conversion of granulite to eclogite, indicated by the complete disappearance of plagioclase, and the formation of a new coarse-grained assemblage that contains omphacite–zoisite–phengite–kyanite–garnet. This omphacite-rich eclogite is strongly foliated and forms a 'matrix' that encloses relict granulite blocks (Fig. 2c). The granulite blocks vary in size, ranging from metre to tens-of-metre scale, and the relict foliation usually cannot be traced smoothly between adjacent blocks. Deflection of the granulite fabric into the foliated eclogite occurs at the margins of the granulite blocks, indicating that plastic deformation was associated with eclogite formation. The stage 3 domains are organized into deformation belts that principally trend 110/20NE, with a subordinate conjugate that trends 050/20SE. Within the ESE trending eclogite belts, the relict granulite blocks commonly have sigmoidal shapes with east–west elongation that suggests bulk dextral top-to-the-east non-coaxial flow (Jolivet *et al.*, 2005; Raimbourg *et al.*, 2005).

Stage 4: In places the strongly foliated eclogite has been overprinted by localized, coarse-grained phengite-rich domains (~40 cm wide at outcrop scale; Fig. 3d), in which earlier formed stage 3 omphacite-rich eclogite has been broken into fragments. These omphacite-rich domains contain euhdral garnet and disseminated omphacite and amphibole, whereas the phengite-rich domains contain minor garnet, omphacite and zoisite. These phengite-rich domains may form the early stages of the amphibolite facies overprint that occurred during

exhumation of the eclogites (Boundy *et al.*, 1992; Kühn, 2002; Kühn *et al.*, 2002; Glodny *et al.*, 2008).

METHODS

Bulk-rock and mineral chemistry

Whole-rock geochemistry for implementation in phase equilibria forward modelling was done at the Department of Earth and Environment, Franklin and Marshall College, Lancaster PA, using Wavelength Dispersive X-ray Fluorescence (WD–XRF) spectrometry. Major elements were analysed on fused disks prepared using a lithium tetraborate flux. Ferric vs ferrous iron content was determined by titration. Whole rock geochemistry in wt% is provided in Table 1.

Mineral composition analyses and elemental X-ray maps were acquired using a CAMECA SXFive electron microprobe at Adelaide Microscopy, University of Adelaide. For elemental analyses, a beam current of 20 nA and accelerating voltage of 15 kV was used. Prior to analysis, calibration was done on an andradite standard, and wavelength dispersive spectrometers (WDS) were used for the analyse of SiO_2, ZrO_2, TiO_2, ZnO, Al_2O_3, Cr_2O_3, FeO, MnO, MgO, CaO, BaO, Na_2O, K_2O, P_2O_5, Cl and F. Element maps were obtained using a beam current of 200 nA and accelerating voltage of 15 kV. Step sizes and dwell times were chosen based on the size of the area mapped and the grain size of the minerals to maximise the resolution. Elements Ca, Fe, Mn and Mg were mapped using WDS, and Al, Si, Ti, K, Na, Zr, Cl, Ce and F were mapped using energy dispersive spectrometers (EDS). Electron backscatter diffraction (EBSD) was used to identify minerals in fine-grained symplectites that

formed during stage 2 replacement of garnet. EBSD mapping was undertaken at the John De Laeter Centre at Curtin University using a Tescan $MIRA_3$. For EBSD analysis samples were polished using 60 nm colloidal silica solution. EBSD maps were collected via the software Aztec (Oxford Instruments). An acceleration voltage and beam current of 20 kv and 15 nA, respectively, were used during acquisition with 50 ms dwell time per pixel. Proportions of minerals were completed by processing the collected EBSD maps of reaction rims of omphacite and garnet. Phengite did not index during EBSD collection and modal proportions have been estimated by EDS phase mapping. Image J was used to calculate the relative modal proportions by colour thresholding.

Phase equilibria forward modelling

Bulk-rock composition determination

Bulk compositions used for phase equilibria forward modelling were determined from whole-rock geochemistry. Weight percent data from whole-rock geochemical analyses (Table 1) were recast in terms of mole percentage of oxide components (e.g. MgO, SiO_2; Table 2) for phase equilibria modelling using THERMOCALC. For samples that had completely recrystallised, the forward modelling calculations used the recast values directly from bulk-rock composition and titration analyses. However, for samples that still contained relicts from the granulitic mineralogy (e.g HOL7C_2014), it was necessary to derive an effective reactive bulk composition prior to using the forward modelling software. This was done by determining the proportion of relict mineralogy and its composition from the electron microprobe data and then subtracting that compositional reservoir from the whole rock geochemical analysis.

P–T pseudosections

Phase equilibria calculations were undertaken using the software program THERMOCALC v.3.33 in the geologically realistic chemical system Na_2O–CaO–K_2O–FeO–MgO–Al_2O_3–SiO_2–H_2O–TiO_2–O, where 'O' is a proxy for Fe_2O_3, using the internally-consistent thermodynamic dataset 'ds5' (filename ds55.txt, 22nd Nov 2003 update of Holland & Powell, 1998). The activity–composition (*a–x*) models used were: amphibole (Diener *et al.*, 2007; Diener & Powell, 2012); clinopyroxenes (Green *et al.*, 2007; Diener & Powell, 2012); chlorite (Holland & Powell, 1998); garnet (White *et al.*, 2007); epidote–clinozoisite (Holland & Powell, 1998); plagioclase and K-feldspar (Holland & Powell, 2003); ilmenite (White *et al.*, 2000); muscovite and paragonite (Coggon & Holland, 2002); chloritoid (White *et al.*, 2000); talc (Holland & Powell, 1998) and biotite (White *et al.*, 2007). The Matlab-based, automated software programme TCInvestigator v2.0 (Pearce *et al.*, 2015) was used to check that the calculated assemblages are the most stable over the modelled parts of *P–T* space during pseudosection construction.

Contouring mineral chemistry and modal proportion

Mineral composition isopleths and normalised modal abundance contours ('mode') were calculated for the forward model using TCInvestigator v2.0 for *P–T* pseudosections. The method used for contouring models is detailed by Pearce *et al.* (2015). Step sizes used for contouring were 0.1 kbar and 1 °C.

RESULTS

Petrography

Four samples were selected to encompass the structural evolution outlined earlier (summary table provided in supporting information). Of these, three samples were subsequently chosen to evaluate the *P–T* evolution of the modified granulites on Holsnøy. Representative photomicrographs of all samples are presented in Fig. 4.

HOL2A_2015 (stage 1)

This sample is from a recrystallised pseudotachylite vein that formed during stage 1. The vein is 4 cm wide and is parallel the granulite foliation and has associated small scale (3 cm by 0.5 cm) injection veins that branch off the main vein. The recrystallised pseudotachylite is fine-grained (<0.1 mm; Fig. 4a) and contains kyanite, omphacite, plagioclase, K-feldspar, zoisite and minor amounts of quartz, rutile and poikiolitic garnet. Clusters of kyanite needles are intergrown with omphacite (Fig. 4a). The matrix also contains domains dominated by K-feldspar that incorporate abundant fine-grained kyanite (Fig. 5a and b). Both in the matrix and within the K-feldspar domains, the kyanite is unoriented. Garnet occurs in minor amounts as highly poikiloblastic grains (Fig. 5c and d) that contain inclusions of plagioclase, K-feldspar, quartz, clinopyroxene and rare rutile. Plagioclase forms abundant polygonal grains (<0.1 mm) in the matrix. Texturally, plagioclase is part of the recrystallised assemblage and is not inferred to be a relict mineral pre-existing from the granulite protolith. The interpreted metamorphic assemblage in the recrystallised pseudotachylite is garnet–kyanite–plagioclase–K-feldspar–omphacite–zoisite–quartz–rutile.

HOL4B_2014 (stage 2)

This sample contains a fine-grained foliated matrix consisting of plagioclase, kyanite, omphacite, phengite and minor quartz (Fig. 4b and 6). The matrix encloses relict garnet and omphacite derived from the granulite protolith. The modal percentage of garnet has been reduced from ~ 18% in the pristine granulite to ~10% in the altered granulite. Garnet is enclosed by thick coronae of fine-grained reaction products that comprise very finely intergrown omphacite–kyanite–zoisite–plagioclase, with coarser individual crystals of kyanite, phengite and omphacite (Fig. 6), and coarser grained zoisite, plagioclase and kyanite comprising the stage 2 shear fabric.

HOL7C_2014 (stage 3)

This sample contains a well-defined stage 3 foliation defined by alignment of zoisite (30%), phengite (10%), elongate omphacite (5%) and minor rutile. X-Ray mapping reveals the presence of trace amounts of kyanite. The foliation encloses garnet grains that range in size from 0.5–2 mm (Fig 4c). The garnets grains are equant and subhedral and display subtle colour variation from relatively pink cores to lighter pink rims (Fig. 4c). Garnet cores contain rare inclusions of spinel, suggesting they are derived from the precursor granulite. Phengite, omphacite and garnet are commonly rimmed by very fine-grained symplectites consisting of amphibole, albitic plagioclase and zoisite (Fig. 4c). The symplectites are typically better formed at grain boundaries that occur at a high angle to the stage 3 foliation. The interpreted peak stage 3 mineral assemblage is zoisite–phengite–omphacite–garnet rim–rutile–kyanite–(H_2O).

HOL13A_2015 (stage 4)

This sample is from a phengite-rich schist that overprints the omphacite–garnet rich eclogite that formed during stage 3. The sample contains medium-grained (0.2–1 mm) garnet,

omphacite (0.2–0.4 mm), zoisite (0.1–0.3 mm), green amphibole (0.2–1 mm) and quartz (0.1–0.2 mm), which are all in contact. These minerals form aggregates that are isolated by very coarse phengite grains (43%; Fig. 4d). Garnet and zoisite also occur within the coarse-grained phengite matrix. The interpreted peak metamorphic assemblage is phengite–garnet–omphacite–rutile–amphibole–quartz–zoisite–(H_2O). The abundance of minerals in volume % is: phengite = 43%; omphacite = 19%; amphibole = 14%; garnet = 11%; zoisite = 8% quartz = 4%; rutile = 0.6%, determined by using pixel counts in Photoshop.

Mineral chemistry

Mineral compositional data were collected from the stage 1 recrystallised pseudotachylite, stage 3 peak eclogite and stage 4 coarse-grained phengite-bearing eclogite. Representative mineral compositions are provided in Table 3, and ranges in mineral chemistry are provided in Table 4.

Garnet

Garnet grains in HOL2A_2015 have weak zoning, with slight core to rim increases in X_{grs} (0.39 to 0.41) and X_{py} (0.12 to 0.16), and corresponding slight decreases in X_{alm} (0.43 to 0.41) and X_{sps} (0.023 to 0.015) (Table 4).

Garnet grains in HOL7C_2014 has a well-defined zonation. Core domains are essentially compositionally unzoned, with X_{grs} ranging between 0.12 and 0.16; X_{py} 0.35–0.38; X_{alm} 0.47–0.49 and X_{sps} 0.015–0.017. The cores are enclosed by a well-defined compositionally contrasting rim that is best expressed by X_{grs} (Fig. 7a and 8a). The rims show slight zoning with X_{grs} decreasing from 0.29 to 0.24 from the interior of the rim to the exterior while X_{py} in

357 the rim increases from 0.22 to 0.27 (Fig. 8a). X_{alm} (0.44) and X_{sps} (0.01) are essentially
358 unzoned (Table 4).
359
360 Garnet grains in HOL13A_2015 shows well-defined compositional zoning (Fig. 7c and d)
361 expressed by a core domain of garnet derived from the protolith and a rim of new garnet (Fig.
362 8b). The cores are compositionally homogenous with X_{grs} content of 0.13–0.16, X_{py} 0.46–
363 0.52, X_{alm} 0.30–0.32 and X_{sps} 0.02–0.03 concentrations (Table 4). The overgrowth is
364 enriched in X_{grs} and X_{alm} with respect to the cores, showing relative increases of around 38%
365 and 20% respectively, and is depleted in X_{py} (Fig. 8b). X_{py} contents, ranging between 0.33
366 and 0.31 with zoning to lower X_{py} content towards the outer margin of the garnet
367 overgrowth. In contrast with X_{py} , X_{alm} concentrations in the garnet overgrowth are
368 comparatively homogeneous. Compositional gradients between cores and overgrowths are
369 steeper for X_{grs} than for X_{py} and X_{alm} (Fig. 8b), suggesting the outer regions of the core
370 domains may have undergone more extensive diffusional modification in Fe and Mg .
371
372 *Phengite*
373 HOL2A_2015 does not contain phengite, however, it is present in the other two samples.
374 HOL7C_2014 contains phengite in the matrix which defines the foliation, together with
375 zoisite and omphacite. Phengite grains in this sample are unzoned, with X_{Mg} values ranging
376 from 0.65 to 0.71 (Table 4).
377 Phengite in HOL13A_2015 is abundant and is formed in the matrix as very coarse grains, but
378 show no zonation. X_{Mg} values for phengite in this sample range from 0.59 to 0.70.
379
380 OMPHACITE

Omphacite grains in HOL2A_2015 occur as intergrowths with kyanite in the matrix. The grain size is too small to identify compositional zoning. They have X_{jad} values of 0.36–0.43; X_{diop} of 0.47–0.53; X_{hed} of 0.11–0.18 and X_{aeg} of 0–0.050 (Table 4).

Compared to HOL2A_2015, HOL7C_2014 contains up to 1.5 mm omphacite grains. The X_{jad} and X_{diop} values range from 0.36–0.41 and 0.46–0.50 respectively. The sample shows significantly lower X_{hed} values (0.01–0.06) and a relative enrichment in X_{aeg} (0.08–0.12) compared to HOL2A_2015 (Table 4).

Omphacite grains in HOL13A_2015 grow in the matrix alongside garnet and amphibole and rarely in the phengite dominated domains. Grains in proximity to the phengite domains usually show slight zonation in both calcium and sodium values, increasing from 0.39 to 0.54 c.pfu and 0.27 to 0.42 c.pfu, respectively, from core to rim, respectively. In general, HOL13A_2015 has X_{jad} values of 0.37–0.39 and X_{diop} of 0.48–0.50 and relatively enriched X_{hed} content of 0.074–0.103 while depleted in X_{aeg} content of 0.029–0.055 (Table 4).

Feldspars

HOL2A_2015 is the only sample to contain feldspars. Plagioclase occurs in the matrix intergrown with kyanite–omphacite clusters and fine-grained zoisite. X_{Ab} values for plagioclase in the sample vary from 0.11 to 0.15 (Table 4). In the same sample, K-feldspar occurs alongside kyanite needles in lense-shaped domains in the matrix (Fig. 5b). X_{or} values of K-feldpar range from 0.84 to 0.88 whereas the Na content is c. 0.20 pfu and Ca content is ~ 0.11 c. pfu (Table 3).

Amphibole

HOL2A_2015 does not contain any amphibole. Amphibole occurs in HOL7C_2014 as very fine-grained symplectites on the margins of garnet and omphacite grains but was too fine-grained to analyse.

In HOL13A_2015, amphibole grain sizes vary from 0.2 mm to 1 mm and the grains are unzoned. In the sample, X_{Mg} values range from 0.63 to 0.71 (Table 4) and Ca content and Na content is 1.58 c. pfu and 1.17 c. pfu respectively (Table 3).

Zoisite

In sample HOL2A_2015, zoisite grows as very fine-grained clusters in the plagioclase, kyanite and omphacite matrix. Zoisite grains in sample HOL2A_2015 has the lowest X_{Fe}^{2+} value (0.34–0.67), but it is relatively enriched in X_{Mg} (1.15–1.97) when compared to zoisite in other samples (Table 4). Ca content is ~ 1.50.

HOL7C_2014 contains elongate zoisite grains which occur in the matrix and, along with phengite and omphacite define the foliation of the sample. Zoisite grains have X_{Fe}^{2+} values in the range of 0.51–0.70 and X_{Mg} values of 0.19–0.36 (Table 4).

In HOL13A_2015, zoisite occurs as coarse grained crystals within the phengite-dominated domain or as smaller (~0.2 mm) grains in the amphibole, omphacite and garnet matrix. The zoisite grains display no zonation and have X_{Fe}^{2+} and X_{Mg} values in the range of 0.65–0.80 and 0.20–0.35, respectively (Table 4).

There appears to be a gradual enrichment in X_{Fe}^{2+} content in zoisite from grains located in the pseudotachylite to the peak eclogite and the retrogressive eclogite as the system evolves.

Pressure–Temperature conditions

P–T pseudosections were calculated for sample HOL2A_2015, HOL7C_2014 and HOL13A_2015 which represent stage 1, stage 3 and stage 4 mineral assemblages,

respectively. These samples collectively span the recorded metamorphic evolution leading up to and immediately post-dating the formation of eclogite on Holsnøy. Thus, they provide a *P–T* framework for the deformation stages and associated fluid–rock interaction.

HOL2A_2015 (recrystallised pseudotachylite; stage 1)

The assemblage within the recrystallised pseudotachylite that formed during stage 1 is garnet–kyanite–plagioclase–K-feldspar–zoisite–quartz–omphacite. The phase equilibria model is shown in Fig. 9 and was calculated using the composition presented in Table 2. The observed assemblage is not well constrained by equilibria modelling as it spans over a large *P–T* space. In the chosen *P–T* window, the peak mineral assemblage occurs at conditions above 10 kbar and 490°C. In an attempt to further constrain the peak field, mineral modes and compositional contours for different minerals were calculated. In this case, the use of isopleths was not useful as they varied parallel to the field boundary of the interpreted peak mineral assemblage (see supporting information). However, garnet and feldpsar compositions can be used to provide an upper limit on the potential *P–T* conditions. Garnet in the assemblage is essentially unzoned, and while this may reflect post growth re-equilibration, the x(g) value range ~0.71–0.73, within the modelled peak assemblage field suggests conditions of around 13.3–15.7 kbar and 630–780 °C. Within the modelled peak assemblage field, K-feldspar composition (X_{Na} ~ 0.140-0.145) coupled with garnet composition, suggest *P–T* conditions of around 15.2 –15.7 kbar at temperatures of ~ 680 °C determined by the overlapping grey regions overlain which represent the two isopleths (individual contour plots provided in supporting information).

HOL7C_2014 (eclogite; stage 3)

The phase equilibria model for HOL7C_2014 shown in Fig. 10 and was calculated using a modified (i.e. with the relict granulite garnet removed; Table 2) bulk composition. The stage 3 peak metamorphic assemblage phengite–garnet–omphacite–rutile–zoisite–kyanite–(H_2O) lies in the *P*–*T* range 21 to >30 kbar and 665 to >800°C. Although we cannot demonstrate that H_2O was present in the peak assemblage, the sample contains pervasive, volumetrically minor retrograde symplectites comprising amphibole and plagioclase that form principally at the expense of omphacite. The presence of this hydrous retrograde assemblage may provide some support for the presence of grain-scale fluid within the peak assemblage.

The modelled peak assemblage *P*–*T* field is large and as such provides only limited constraints. However, the peak *P*–*T* conditions estimates can be improved using contours of mineral abundance, in concert with measured mineral chemistry. The measured compositional isopleth corresponding to z(g) of 0.26-0.29, x(o) of 0.10–0.13 and j(o) =of 0.48–0.50 are overlain as faded grey areas on Fig. 10 (individual contours are provided in supporting information). Although these compositions cover a large portion of the *P*–*T* model, they do intersect within the peak assemblage field. Combining the intersections of all the plotted values of isopleths, the peak *P*–*T* conditions for this sample can be constrained more tightly to approximately 21–22 kbar and 670–690 °C.

HOL13A_2015 (phengite-rich eclogite; stage 4)

The model in Fig. 11 was calculated using the whole-rock composition presented in Table 2 for the retrogressed, phengite-rich eclogite. The peak metamorphic assemblage phengite–garnet–omphacite–rutile–amphibole– zoisite–quartz–(H_2O) occurs in the *P*–*T* range 14.0–17.5 kbar and 650–760 °C. To further constrain the peak conditions, the modal proportions of

phengite, omphacite, quartz and zoisite within the peak assemblage and were plotted as grey shaded regions on Fig. 11, where they coincide in the top left corner of the peak mineral assemblage field. The more tightly constrained *P–T* conditions occur in the range of 16–17 kbar and 680–700 °C.

DISCUSSION

The aim of this study is to provide a *P–T* framework (i.e. burial and exhumation) for the fluid assisted conversion of granulite to eclogite recorded on Holsnøy Island in the northern Bergen Arcs. The *P–T* conditions presented here are linked to the different stages of the deformational evolution that have been described in detail by Austrheim (2013). However, before linking the different *P–T* conditions that were calculated in this study, it is essential to assess the validity of phase equilibria modelling to the rocks on Holsnøy Island.

Application of phase equilibria modelling on Holsnøy Island

The underlying assumption of the mineral equilibria modelling shown in the previous sections is that mineral growth occurs via equilibrium processes within a constant bulk rock composition. Indeed, it is this notion of a closed system requirement that underlies a duality in thinking when applying mineral equilibria modelling to mineral assemblages. For example, the application of melt reintegration modelling to investigate the petrological evolution of granulite(Brown, 2007; Anderson *et al.*, 2012; Korhonen *et al.*, 2013) seeks to adjust the bulk composition of a rock via sequential addition of melt to attempt to explain the development of minerals that may have formed before the currently preserved bulk composition of the rock was created. In this way open system behaviour is addressed in a mechanical and user-defined manner.

For the rocks exposed on Holsnøy, it is evident that open system behaviour has played an essential role in the transformation of anorthositic granulite to eclogite (Austrheim, 2013). At the outcrop scale, the manifestation of this open system behaviour is dramatic, with the formation of hydrous high-*P* amphibolite and eclogite domains at the expense of garnet–clinopyroxene–orthopyroxene-bearing anorthosite. However, despite clear petrological differences between the protolith and the fluid affected rocks, there is surprisingly little difference in the major element chemistry between the eclogite domains and their wall rocks (Fig. 12; Kühn, 2002; Schneider *et al.*, 2007). For the samples used in this study, major element comparisons between the protolith granulite and the immediately adjacent sampled recrystallised rock are shown in Fig. 12. For the recrystallised pseudotachylite sample HOL2A_2015, it evident that there is little compositional change compared to the protolithic granulite, suggesting the assumption of an invariant bulk composition during rock recrystallization is valid. However, for the peak metamorphic eclogite sample HOL7C_2014 and interpreted retrograde sample HOL13A_2015, it is evident that compositional changes have occurred. For HOL7C_2015, the eclogite is less silicious and more calcic than its protolith, although based on the loss of ignition (LOI; Table 1; Fig. 12), is not significantly more hydrated. In HOL13A_2015, based on LOI, it the sample is much more hydrous than its protolith, as well as significantly more Fe-rich and potassic.

It is beyond the scope of this paper to undertake a detailed analysis of the chemical changes associated with the conversion of granulite to eclogite. However, the critical question is to what extent the rock composition changed while the petrologically observed mineral assemblage formed. Schneider *et al.* (2007) undertook an evaluation of scales of chemical equilibrium within samples that correspond to our stage 2 and stage 3 recrystallisation, concluding that samples at thin section scale did not operate as an equilibrium system. This

522 was most evident in the sample that corresponds to stage 2, which displays complex
523 symplectitic coronas around garnet that reflect microscale chemical domains. Because of
524 these textural complexities and their associated microchemical domains, we chose not to
525 model the stage 2 assemblages. However, for a sample of omphacite-rich eclogite which
526 corresponds to our stage 3 assemblage Schneider *et al.* (2007) determined that mineral
527 compositions showed comparatively little variation. Notably, compositional variation in
528 minerals like phengite was associated with the formation of volumetrically minor secondary
529 retrograde phengite, rather than the formation of prograde micro-chemical domains. In our
530 stage 3 sample, aside from garnet, we also find comparatively little compositional variation in
531 minerals.
532
533 In the case of recrystallised pseudotachylite sample HOL2A_2015, it appears that little
534 chemical change occurred between the protolith and the recrystallised rock. In eclogite
535 sample HOL7C_2014, there is a strong foliation with a distributed mineral assemblage that
536 shows no textural evidence for sequential or spatially heterogeneous mineral growth, veining,
537 or other textural criteria that would suggest a progressive change in bulk composition
538 occurred during the formation of the currently preserved mineral assemblage. Aside from
539 compositional zoning in the garnet overgrowths surrounding relict protolith garnet, which
540 could reflect the evolving *P–T* conditions, minerals such as omphacite, zoisite and phengite
541 show little compositional variation. We suggest that the lack of obvious sequential mineral
542 growth and compositional zonation reflects a comparatively static bulk composition during
543 the growth of the preserved mineral assemblage. Similarly in HOL13A_2015, there are no
544 systematic mineral textures that point to preservation of fluid-infiltration driven reaction
545 fronts, and the minerals (aside from the relict granulite garnet cores), show little

546 zoning. Again we suggest this could be interpreted to reflect a comparatively static bulk
547 composition during the formation of the mineral assemblage in the sample.
548
549 Therefore, while we acknowledge that open system behaviour clearly drove the transition of
550 granulite to eclogite, the evidence points to open system processes either establishing an
551 altered bulk composition prior to the growth of the mineral assemblages, or to primarily
552 modifying the hydrous content of the rock (e.g. Boundy *et al.*, 1997; Bjørnerud *et al.*, 2002;
553 Kühn, 2002; Schneider *et al.*, 2007). In this context, Austrheim (1990), Boundy *et al.* (1992),
554 Austrheim *et al.* (1997) and Bjørnerud *et al.* (2002) suggested that the conversion of
555 anhydrous granulite into eclogite was rapid in terms of rate process (see also Camacho *et al.*,
556 2005). Therefore, we take the axiom that while some bulk rock compositional change may
557 have occurred subsequent to the mineral growth in the samples we have selected, insufficient
558 bulk rock compositional change occurred to dis-establish the mineral assemblages. Indeed,
559 the character of the Holsnøy granulite to eclogite transition points to a fluid triggered, but
560 typically locally fluid abandoned system, leaving stranded preserved compositional domains
561 that are effectively static snapshots of open system modification (see below). Therefore, for
562 the purposes of *P–T* forward modelling, the samples as preserved are effectively quasi-closed
563 systems, and the application of phase equilibria modelling is a valid approach to evaluate the
564 *P–T* conditions of the system, via the careful selection of samples constrained by field
565 relationships that indicate the assemblages formed at different times in the thermobarometric
566 evolution.
567
568 A second issue that must be addressed in applying mineral equilibria modelling is the
569 selection of an appropriate bulk composition. Where a rock is texturally homogeneous, and
570 contains unzoned minerals, the choice of an appropriate bulk composition is straightforward

(e.g. Kelsey & Hand, 2015). However, in rocks that are texturally complex, or contain relicts of unreacted protolith minerals, the selection of an appropriate bulk composition is less straightforward (Stüwe, 1997; Kelsey & Hand, 2015; Guevara & Caddick, 2016).

For the rocks on Holsnøy Island, while stage 3 mineral assemblages are mesoscopically and microscopically homogeneous, compositional imaging (e.g. Fig. 7a and b) shows that the garnets contain a distinct core and rim compositional morphology. This has also been described by numerous previous studies (e.g. Austrheim & Griffin, 1985; Pollok *et al.*, 2008; Russell *et al.*, 2012). Petrographically, some of the garnet cores in the altered samples contain inclusions of spinel (supplementary data). Spinel inclusions within garnet are sparse, but widespread within the granulitic protolith. Therefore, we interpret the compositionally distinct garnet cores in eclogite to be relict domains inherited from the granulite protolith. The distinct compositional contrast between the garnet cores and overgrowths suggests the garnets did not contribute significantly to the effective reactive bulk composition comprising the stage 3 eclogite assemblages.

In an attempt to investigate if incorporation of the relict garnet cores exerts a significant influence on the modelled phase relations, the unmodified whole-rock composition for HOL7C_2014 (Table 2; HOL7C*) was modelled and a compared with a modified composition where the garnet cores have been removed (also Table 2). Removal of the garnet cores was done in the admittedly simplistic way of determining the proportion of garnet cores in thin sections of the sample using Adobe Photoshop pixel counting with photographic images, X-Ray compositional maps and electron microprobe data followed by: (1) assuming the garnets are spherical and on average sectioned through their centres; (2) determining the 2D portion of garnet core to rim, and converting that to a volumetric ratio;

(3) determining the proportional integrated compositional reservoir in the garnet cores by combining their volumetric proportion and their average composition; (4) Subtracting this from the measured whole-rock composition; and (5) assuming there is negligible growth of new grains of purely eclogitic garnets.

The comparison between two the bulk compositions is shown in Fig. 13. It shows the difference in the abundances of garnet throughout the modelled *P–T* window for the two bulk compositions. It is evident there is only a narrow domain in *P–T* space where the difference in abundance is low (pale blue strip extending across the model from top left corner to bottom right). The peak fields for the two modelled composition are also plotted on Fig. 13 and show a significant difference, which supports the notion that modelling a simple bulk rock composition, when it is evident there are compositionally refractory domains, may give rise to biased *P–T* estimations (Marmo *et al.*, 2002; Palin *et al.*, 2015; Ren *et al.*, 2016). This highlights a general principal in *P–T* modelling that the modelled bulk composition should be defined only by the minerals that formed from the effective chemical system (Stüwe, 1997; Kelsey & Hand, 2015). In the case of stage 3 mineral assemblages on Holsnøy Island, we suggest that the bulk composition defined by the homogeneously distributed assemblage, including the garnet overgrowths is a defensible bulk composition for modelling.

It is evident from Fig. 7c and d that the retrogressed phengite-rich sample HOL13A_2015 contains relict domains within garnet that are probably inherited from the granulite protolith. However, in contrast to HOL7C_2014, the garnets in HOL13A_2015 are much smaller (typically 0.2–0.9 mm in diameter), the compositional zoning are more diffused, and the rim domains are correspondingly a much greater proportion of the overall garnet volume and composition compared with HOL7C_2014. Additionally, garnet only comprises ~ 11% of

621 the assemblage, making the relict cores a small proportion of the overall bulk composition.
622 For this reason we have taken the bulk thin-section rock block geochemistry as a reasonable
623 approximation of the effective bulk composition of the sample.

624 ***P–T* evolution**

625 Mineral equilibria forward modelling has provided the basis for erecting a framework for the
626 prograde, peak and retrograde *P–T* conditions of the eclogitisation process recorded on
627 Holsnøy Island, i.e. define the *P–T* path of the process. The inferred *P–T* conditions for the
628 recrystallised pseudotachylite, eclogite and retrogressed eclogite are summarised in Fig.14.
629 Our peak P–T conditions are broadly similar to those derived from conventional
630 thermobarometry and average *P–T* approaches (Jamtveit *et al.*, 1990; Raimbourg *et al.*,
631 2007). However, we note that in several of these earlier studies (e.g. Austrheim & Griffin,
632 1985; Mattey *et al.*, 1994), plagioclase-bearing equilibria were used even though the peak
633 eclogite assemblage does not contain plagioclase.
634
635 The oldest structures that overprint the Neoproterozoic granulite are a series of small scale
636 pseudotachylites and associated brittle structures. The pseudotachylites have recrystallised to
637 fine-grained metamorphic mineral assemblages (discussed previously). These recrystallised
638 pseudotachylites were the focus of previous studies (Austrheim & Boundy, 1994; Austrheim
639 *et al.*, 1996; Austrheim *et al.*, 2017), and were interpreted to be the record of seismic events
640 that occurred at eclogite facies at *P–T* conditions of 18–19 kbar and ~800 °C during the
641 Caledonian Orogeny. These conditions were calculated using conventional thermobarometry
642 on omphacite–garnet pairs. The formation of the pseudotachylites was interpreted to be the
643 result of fast relaxation of stresses owing to fluid induced eclogitisation of the granulite
644 (Austrheim & Boundy, 1994) as the volume of the domains decreased. However, based on

field relationships and mineral assemblages within the *recrystallised* pseudotachylites, and the fact that the age of the brittle deformation is unknown, it is difficult to unambiguously deduce whether they were formed during the later stage of the Grenvillian Orogeny, the early stages of the Caledonian Orogeny or in the interval between the two. The critical *P–T* information provided by the mineral assemblage within the recrystallised pseudotachylite is that it places upper constraints on the depth of the brittle deformation, which is not necessarily a close constraint for the depth of the deformation itself. Thus, the mineral assemblage garnet–K-feldspar–plagioclase–kyanite–quartz–omphacite–zoisite–rutile in the recrystallised pseudotachylite does not provide precise *P–T* constraints. However, based on the relative timing of the pseudotachylite formation (described previously) and the *P–T* conditions of the complete conversion of the granulite to eclogite (see below), we conservatively suggest that the *P–T* conditions at which the pseudotachylite recrystallised at was no greater than that modelled for the peak metamorphic eclogites. In this case, the maximum *P–T* for the formation of pseudotachylites would be less than 22 kbar and 700 °C. This is reflected in the model (Fig. 9) where a *P–T* range of 15.2–15.7 kbar and 675–685 °C was calculated. This estimate contrasts with a number of previous worker (e.g. Austrheim & Boundy, 1994; Lund *et al.*, 2004). Additionally, the presence of abundant sodic plagioclase in the recrystallised pseudotachylite (Table 4) suggests that it has recrystallised at high-pressure amphibolite or granulite grade conditions (Ringwood & Green, 1966; Zhang *et al.*, 2003; De Paoli *et al.*, 2009), rather than eclogite facies conditions as previously suggested (Austrheim & Boundy, 1994). Irrespective, aside from a maximum possible pressure of recrystallisation, there are no constraints on the pressure (depth) of the pseudotachylite formation, and no evidence they formed at eclogite facies conditions.

Based on the maximum pressure constraint, the notion that pseudotachylite recrystallisation occurred under comparatively low-*P* conditions is consistent with the overprinting structural

relationships and metamorphic assemblages. The recrystallised pseudotachylites are overprinted by small-scale shear zones (stage 2) associated with hydrous alteration that defines the classic metasomatic alteration on Holsnøy (Fig. 3b) that has been described by numerous authors (e.g. Jamtveit *et al.*, 1990; Van Wyck *et al.*, 1996; Austrheim, 2013). Although this metasomatism is associated with the growth of sodic clinopyroxene, a notable feature in these altered domains is the modal decrease of garnet compared to the granulite protolith. These alteration zones also commonly contain abundant albitic plagioclase that forms part of the recrystallised assemblage, and so stage 2 shear zones do not define eclogite assemblages (Fig 6). Therefore, it is unlikely that the pseudotachylites formed at eclogite facies conditions. A notable feature of stage 1 and stage 2 deformation is the extensive fracturing of garnet grains in the granulitic wall rock and sheared fabric of the altered domain, respectively. These fractured garnets and their compositional response to the high-*P* reworking have been the focus of several studies (Jamtveit *et al.*, 1990; Erambert & Austrheim, 1993; Raimbourg *et al.*, 2007; see below).

Overprinting the stage 2 albitic plagioclase-bearing alteration zones are domains of pervasively recrystallised plagioclase-free rock (stage 3) with the metamorphic assemblage phengite–garnet–omphacite–rutile–kyanite–zoisite–(H_2O), which defines a true eclogite assemblage. These domains form kilometre-scale zones in which an anastomosing foliation envelops relict granulite blocks, creating a structural domain previously referred to as the eclogite "breccia" (Austrheim, 2013). These "breccia" domains are marginal to a system of high-strain zones that were interpreted to have been formed during NW–SE tectonic transport (Raimbourg *et al.*, 2005). Peak metamorphic conditions modelled for eclogite (HOL7C_2014) in these high-strain zones are constrained at 21–22 kbar and 670–690°C (Fig. 10). These new estimates are in general agreement with the higher-*P* and lower-*T* estimates

made from conventional thermobarometry (18–21 kbar and 650–800 °C; (Austrheim & Griffin, 1985; Jamtveit *et al.*, 1990; Pollok *et al.*, 2008; Austrheim, 2013). However, there are numerous pitfalls associated with using conventional thermobarometry. These include: (1) re-equilibration of mineral compositions with cooling; (2) accounting for Fe^{3+} in minerals (e.g. clinopyroxene), affecting the apparent Fe-Mg K_D with minerals such as garnet; (3) only using a small subset of the total mineral assemblage for thermobarometry; (4) not knowing whether the derived *P–T* conditions actually occur within the stability field of the assemblage itself, and (5) the circular need to estimate *P* in order to calculate *T* and vice versa (Kelsey *et al.*, 2003; Powell & Holland, 2008). However, the general agreement between conventional *P–T* calculations which use small-scale mineral pairs (effectively microdomains) and our more general bulk compositionally based forward *P–T* modelling suggests the rock system is compositionally and mineralogically amenable to *P–T* modelling.

The large high-strain stage 3 domains are locally overprinted by smaller scale domains that contain coarse-grained phengite-rich mineral assemblages. Forward modelling of sample HOL13A_2015 (Fig. 11) which was selected from one of these zones suggests that this post-peak, fluid-rich assemblage recrystallised at around 16–17 kbar and 680–700 °C. The calculated conditions are close to the estimates of peak *P–T* conditions from earlier studies (Austrheim & Griffin, 1985) for high-*P* retrogression of the eclogites.

While it cannot be unequivocally established, the precedent of existing studies (Jamtveit *et al.*, 1990; Austrheim & Boundy, 1994; Austrheim, 2013) suggests that the modelled mineral assemblages all formed during the Caledonian Orogeny between c. 460–430 Ma. Assuming this interpretation is valid, the *P–T* conditions recorded by each of the three samples are linked in sequence by a simple *P–T* evolution path. The interpreted *P–T* path for the Holsnøy

eclogites and the associated metasomatic process is shown in Fig. 14 and defines a clockwise evolution. If the retrograde path continued along a trajectory of decreasing pressure but with gradually increasing cooling, the rocks would track into the amphibolite facies. Amphibolite facies reworking of eclogites is documented elsewhere in the Bergen arcs (Andersen *et al.*, 1991b; Andersen *et al.*, 1991a; Boundy *et al.*, 1992; Engvik *et al.*, 2000; Bingen *et al.*, 2001; Raimbourg *et al.*, 2005; Glodny *et al.*, 2008). In the face of the record of this amphibolite facies reworking, the excellent preservation of the granulite to eclogite transition on northeastern Holsnøy likely reflects a domain that saw fluid flow in the early to mid-stage of the Caledonian Orogeny but then was abandoned by fluids, allowing for its preservation.

P–T **constraints and fluid infiltration**

A large number of studies have focussed on the role of fluids in facilitating the transition of granulite to eclogite in the Bergen Arcs, and on Holsnøy in particular (e.g. Austrheim, 1987; Jamtveit *et al.*, 1990; Van Wyck *et al.*, 1996; Boundy *et al.*, 1997; Austrheim, 1998; Kühn, 2002; Glodny *et al.*, 2008; Austrheim, 2013). However, the majority of these studies have not evaluated the fluid ingress in a progressive context. Instead fluid, ingress has generally been considered to have occurred at around peak conditions and continued during the retrograde evolution, leading to the development of extensively developed retrograde amphibolite facies mineral assemblages (Bingen *et al.*, 2004; Raimbourg *et al.*, 2005; Glodny *et al.*, 2008). Fluid ingress appears to have been channelized along zones of fracture- and shear zone- hosted permeability leading to a volume of at least several cubic kilometres of infiltrated rocks (Jamtveit *et al.*, 1990; Austrheim, 2013). However, the generally low variance nature of the mineral assemblages and the limited geochemical changes between the protoliths and the recrystallised rocks suggests that fluid–rock ratios were generally low.

744 This study does not focus on the fluid–rock interaction specifically or the source of the fluids,
745 but, implicit in the descriptions of the metamorphic assemblages that characterise structural
746 stages 1–4 is that fluid ingress began on the burial path before the peak metamorphic
747 eclogitic facies assemblages formed. This is evident from mineral assemblages developed
748 within the recrystallised pseudotachylite that formed during structural stage 1. These
749 assemblages are characterised by the development of phengite and zoisite, with zoisite
750 forming a locally volumetrically large component of the mineral assemblage. While the *P*–*T*
751 constraints on the development of the mineral assemblages within the recrystallised
752 pseudotachylite are not as precise as would be ideal, within the probable range of temperature
753 constraints, fluid was apparently available in the comparatively early stages of prograde
754 burial to create hydrated mineral assemblages. Furthermore, based on the presence of
755 abundant recrystallised plagioclase, fluid ingress occurred before the rocks entered the
756 petrological eclogite facies.
757
758 Structurally, stage 2 is characterised by the formation of narrow domains of altered granulite
759 may flank thin quartz veins, or occupy the cores of meso-scale low strain kink bands and
760 minor ductile shear zones (Austrheim, 2013). In this study we have not focussed on this
761 stage of recrystallization. However, petrologically stage 2 is characterised by the breakdown
762 of garnet inherited from the granulite protolith to fine-grained symplectic assemblages
763 consisting of a potassic assemblage omphacite–zoisite–phengite–kyanite (Fig. 6); that occur
764 within a matrix of foliated zoisite and recrystallised plagioclase. Modally within these
765 reaction textures, hydrous minerals comprise around 20 % of the replacement minerals, and
766 the surrounding matrix may contain up to 25 % zoisite. The modal abundance of garnet
767 typically undergoes ~30–40 % reduction relative to the protolith granulite (Fig. 15a). As with

768 the recrystallised stage 1 pseudotachylite assemblages, petrologically the stage 2 assemblages
769 are not eclogitic because they contain abundant recrystallised plagioclase.
770
771 Although the bulk compositions of fluid-affected rocks of stage 2 and stage 3 (peak eclogite
772 stage; sample HOL7C_2014) are different, the difference is not significant (Table 1; Fig. 12).
773 This means that the general mineralogical relationships and associated trends in garnet modal
774 abundance proportions, from HOL7C_2014 shown in Fig. 15b could act as a general guide to
775 the metamorphic character of stage 2. For example, in most metamorphic systems, the modal
776 proportion of garnet is strongly positively correlated with pressure (Tracy & Robinson, 1976;
777 Spear *et al.*, 1984; Caddick *et al.*, 2010) as shown in Fig.15b. Using Fig. 15 as a proxy and
778 the fact that the transition of the granulite to eclogite was facilitated by the presence of fluid
779 (Andersen *et al.*, 1991c; Austrheim, 2013), for garnet abundance to significantly reduce
780 during stage 2 (Fig. 8b and Fig. 15a), the fluid–rock interaction probably occurred at
781 pressures well below the inferred peak pressures of ~22 kbar derived from the stage 3 mineral
782 assemblage, where garnet abundance is low (Fig. 15b).
783
784 Stage 3 assemblages form the peak metamorphic (eclogite) assemblages preserved on
785 Holsnøy. They are characterised by true eclogite assemblages that lack plagioclase, but still
786 contain abundant phengite and zoisite. Unlike the preceding stage 2 assemblages, stage 3
787 assemblages show clear evidence for the growth of new garnet which forms rims on the relict
788 protolith garnets (Fig. 7b), thus reversing the reduction in garnet modes evident at stage 2.
789 The progressive structural and mineralogical development culminating in the development of
790 hydrated plagioclase-free stage 3 mineral assemblages implies that fluid infiltration occurred
791 either continuously or sporadically during the prograde burial, once the granulitic slab had
792 approximately reached mantle depths. It is difficult to unambiguously demonstrate that

progressively more channelised fluid flow culminated in the development of the peak stage 3 assemblages (as opposed to a new and comparatively high flux fluid ingress). However, even within domains dominated by stage 3 assemblages, relict granulite blocks have gradational margins with the enclosing eclogite, and internally contain stage 2 structural features and assemblages (Fig. 2c). This suggests that stage 3 assemblages may have progressively developed as fluid flow either increased, or became more structurally focused. The preservation of stage 2 assemblages in close proximity to stage 3 assemblages also implies that fluid infiltration was not pervasive. Rather it suggests that fluid ingress was channelized and/or approximately balanced by consumption to form the hydrous mineral assemblages, leaving little fluid to catalyse stalled stage 2 reaction assemblages.

The excellent preservation of the granulitic protolith away from areas of obvious fluid mediated recrystallisation highlights the importance of the catalysing effects of fluids. This is further underscored by the comparatively minor bulk rock compositional changes associated with fluid ingress (Schneider *et al.*, 2007; Table 1 and Fig. 12). The preservation of the protoliths in areas of comparatively minor (or essentially non-existent) fluid ingress, illuminates an important facet of the Holsnøy system, that is, if fluid ingress ceased into a specific volume, the affected volume essentially froze in its mineralogical state, thereby preserving a snap shot of the system at a point in time. This means that judicious sampling could effectively discretise the prograde and conceivably the retrograde evolution.

The source(s) of the fluid are beyond the scope of this study. However, based on an assumed mantle reservoir of around $\delta^{13}C$ -5 ‰ and a shift from comparatively heavy to lighter carbon isotopes accompanying eclogitising of the granulites, Mattey *et al.* (1994) suggested the source of fluid was the dehydration of sedimentary rocks below the granulites. A number of studies (see review by Deines, 2002) have also shown that mantle carbon isotopes are essentially bimodal in composition with peaks at around $\delta^{13}C$ -5 ‰ and $\delta^{13}C$ -25 ‰, indicating that the recorded carbon isotope shift associated with the eclogitising fluids on Holsnøy do not preclude a mantle source for the fluids. However, the evidence points to a system that underwent protracted fluid–rock interaction as expressed by the record of fluid–rock interaction that began during prograde burial. This suggests that fluids were, potentially, derived from a source that underwent progressive dehydration, and therefore a source that accompanied the granulites during subduction.

Duration of fluid-rock interaction

Erambert and Austrheim (1993) and Raimbourg *et al.* (2007) used the diffusional response of garnet in the Lindås Nappe to explore the potential timescales associated with the conversion of the anorthositic granulite to eclogite. They identified two different modes of garnet responses; (1) protolith garnets that underwent fracturing and diffusional modification and (2) garnet that grew during high-*P* metamorphism. Fracturing of garnet was associated with the development of stage 1 and stage 2 structures that formed during the prograde evolution, whereas new garnet growth occurred during stage 3, and overprinted fractured garnets that had already been diffusionally modified (Raimbourg *et al.*, 2007). Using a range of different estimates for garnet diffusion coefficients and an assumed temperature of 700°C, calculated timescales for diffusion range between 0.7–12 Ma (Erambert & Austrheim, 1993; Raimbourg *et al.*, 2007), which provides a guide to the potential duration between the time garnets

838 fractured and the time that new garnet grew during the metamorphic peak. Modelling of the
839 compositional response of the new grown peak garnet suggested fast retrograde time scales.
840 According to Raimbourg *et al.* (2007), for the peak and retrograde evolution, the rocks could
841 not have resided at temperatures in excess of 650 °C for more than ~ 150 ky based on the
842 garnet diffusion coefficients of (Ganguly *et al.*, 1998). Even shorter timescales are required
843 for the coefficients of Carlson (2006). Based on the diffusional response of garnet, the bulk
844 of the fluid rock interaction appears to have occurred on times of no more than several
845 million years, and potentially significantly less. The apparent time scales of the retrograde
846 evolution imply rapid retrograde pressure change. *P–T* estimates for post peak eclogite
847 retrogression, amphibolite-grade assemblages suggest conditions around 620–650 °C and 10
848 kbar (Kühn, 2002). If these retrograde conditions were encountered on the post peak path on
849 the time scales implied by garnet diffusional modelling, it suggests the retrograde evolution
850 of the Lindås Nappe experienced extremely rapid pressure change.

851 **CONCLUSIONS**

852 Holsnøy Island in the Bergen Arcs, Norway, contains a well-documented record of fluid
853 catalysed conversion of early Neoproterozoic nominally anhydrous anorthositic granulite to
854 hydrous eclogite associated with Caledonian-aged (c. 450 Ma) subduction of continental
855 crust. Prograde burial is recorded by a sequence of mineral assemblages that record the
856 progressive loss of plagioclase as burial and hydration proceeded. The earliest recorded
857 prograde mineral assemblages formed during the recrystallization of structurally early
858 pseudotachylite. *P–T* modelling shows the assemblage is not particularly *P–T* sensitive, but
859 is likely to have recrystallised at conditions between 15.2–15.7 kbar at 675–685 °C,
860 suggesting that the pseudotachylite must have formed below these conditions. The
861 recrystallised pseudotachylite was overprinted by low-strain deformation zones associated

with prominent hydrous recrystallisation. The peak assemblages are recorded by kilometre-scale domains of foliated eclogite that formed around 22 kbar and 680 °C. The peak assemblages are overprinted by localised phengite-rich assemblages that formed during high-*T* retrogression at around 16–17 kbar and 680–700 °C. The sequentially developed mineral assemblages and *P*–*T* constraints show that the granulite experienced long-lived (prograde, peak and retrograde) fluid driven recrystallisation during the subduction of anorthositic crust. The availability of fluid during burial and exhumation implies a fluid source that was able to progressively dehydrate during subduction of the granulites. Potentially this fluid source was derived from sedimentary sequences elsewhere in the subduction channel.

ACKNOWLEDGMENTS

Luke Hersey, Curtin University, is thanked for his help with the mapping part of the project. Ben Wade, Angus Netting and Aoife McFadden, Adelaide Microscopy, are also thanked for their assistance with the electron microprobe and SEM. Lastly, many thanks to Stephanie Wikan Tyiasning and Nigel Rees, University of Adelaide, for their invaluable help with Matlab and Python, respectively.

Figure 1. Geological map of northern Holsnøy island, modified from Austrheim *et al.* (1996) and Boundy *et al.* (1992). Sample locations are indicated as red stars.

Figure 2. Detailed outcrop-scale maps showing the relationship between different lithological domains on Holsnøy Island. (a) Pseudotachylite veins cross-cutting the foliation of granulite in stage 1 and later overprinted by partially hydrated shear zone. (b) Structural features in stage 2 of deformation, namely the formation of fractures and discrete shear zones which are both accompanied by fluid alteration. (c) The formation of granulite blocks (previously described as the granulite 'breccia') enclosed by highly sheared eclogite in stage 3 of deformation. Map details are provided in supporting information.

Figure 3. Field photographs illustrating the different stages of deformation. (a) Pseudotachylite outline in red overprinted by a partially hydrated shear zone (grey zone on right of the picture) during stage 1 of deformation. The boundary between the granulite and partially hydrated zone is outlined in green. Camera cap as scale is 60 mm (b) Small-scale partially hydrated shear zone (denoted grey zone) in stage 2. Displacement of coronitic bands, up to 1 m shown by the yellow dashed lines in and out of the shear zone. Scale bar is 11 mm. (c) Granulite blocks (circled) sitting in extensively sheared eclogite forme during stage 3 of deformation. Foliation in individual granulite blocks cannot be followed from one block to another one (highlighted in yellow dashed line). (d) Retrogressive phengite-rich eclogite (pale strip in the middle of photo) overprinting eclogite (dark green domain on top left of photo). Pink pen tip at bottom right of picture for scale.

Figure 4. Photomicrographs showing the textures and mineral relationships in the different samples. (a) Sample HOL2A_2015 is a recrystallised pseudotachylite that represents stage 1 of deformation. The matrix comprises very fine-grained light-coloured plagioclase and darker omphacite and kyanite intergrowths enclosing garnet poikiloblasts and lense-shaped domains of intergrown K-feldspar and kyanite. (b) Sample HOL4B_2014 represents stage 2 of deformation. Relict granulitic garnet grains are enclosed by fine-grained plagioclase kyanite, omphacite and phengite-bearing symplectites replacing garnet grains. The light-coloured matrix comprises of plagioclase and zoisite. (c) Sample HOL7C_2014 occurs in stage 3 deformation. Garnet with apparent zoning sits in a matrix of omphacite, zoisite and phengite with growth of amphibole-rich symplectites at garnet-omphacite grain boundaries. (d) Sample HOL13A_2015 represents stage 4 of deformation. A coarse-grained phengite matrix separates amphibole–omphacite–zoisite–garnet–quartz–bearing domains into isolated aggregates.

Figure 5. Representative electron microprobe X-ray maps of two regions in sample HOL2A_2015. Scalebar at the bottom of all maps is 200μm. On the colour scale, white represents relatively high abundance of an element while black represents relatively low abundance. (a) Aluminium map highlighting kyanite, which appears as bright yellow needles. (b) Potassium map used highlighting K-feldspar, which form the two bright pods, with inclusions of kyanite needles within them. (c) Silicon map of a garnet in sample HOL2A_2015, showing small grains of quartz in the matrix and as inclusions in the garnet rim. (d) Manganese map of a garnet HOL2A_2015 showing minor Mn zonation with relative enrichment in the core compared to rim.

Figure 6. EBSD image of garnet breakdown texture in HOL4A_2014, representing stage 2 of deformation. In this sample, garnet breaks down owing to fluid infiltration to form a symplectite rim comprising omphacite, kyanite, zoisite, phengite and plagioclase. The matrix is predominantly made up of plagioclase, zoisite, kyanite and minor quartz. Zoisite, kyanite and plagioclase define the foliation, wrapping around the garnet and symplectite.

Figure 7. Electron microprobe X-ray maps of garnets in HOL7C_2014 (top) and HOL13A_2015 (bottom). Scalebar at the bottom of each map is 2mm. On the colour scale, white represents relatively high abundance of an element while black represents relatively low abundance. (a) X-ray map of calcium in HOL7C_2014. There is a very sharp boundary between the core and rim, with a distinct enrichment in Ca in the rim of garnet grains. Garnet cores are interpreted to be relict from the granulite and make up approximately 75 vol. % of garnet grains. (b) Magnesium X-ray map of garnet in HOL7C_2014. Garnet grains show a general decrease in Mg content from core to rim. (c) Calcium X-ray map of garnet grains in HOL13A_2015, which have smaller cores than those in HOL7C_2014, show similar increase in Ca content at the rims. (d) Magnesium X-ray map of garnet grains in HOL13A_2015. As in HOL7C_2014, there is a general decrease of Mg content from core to rim, however, the core-rim boundary is less sharp.

Figure 8. Zonation profile of garnet grains in (a) HOL7C_2014 and (b) HOL13A_2015. In both samples, X_{grs} content seems to increase from core to rim, X_{py} decreasing and X_{sps} increasing. X_{alm} decreases from core to rim in HOL7C_2014, whereas it increases in HOL13A_2015.

Figure 9. (a) Calculated *P–T* pseudosection for sample HOL2C_2015. The bulk composition at the top of the model is expressed as mol %. The white fields have a variance of two whereas the darkest shade of blue indicates variance of six. Mineral abbreviations are from Holland and Powell (1998).

*very small fields are not labelled.

The bold outline indicates the peak mineral assemblage and the red star designates approximate *P–T* conditions. The grey shaded regions represent the contour ranges for garnet composition *x*(g) of 0.71-0.73) and K-feldspar ranges (X_{Na} ~ 0.140-0.145), used to further constrain the peak conditions. Peak conditions were selected where the two contours overlap, as indicated by the red star.

Figure 10. Calculated *P–T* pseudosection for modified bulk composition (relict granulitic garnet removed) of sample HOL7C_2014 (Table 2). The bulk composition at the top of the model is expressed as mol %. The white fields have a variance of two whereas the darkest shade of blue indicates variance of six. Mineral abbreviations are from Holland and Powell (1998).

*very small fields were not labelled.

The bold outline indicates the peak mineral assemblage. For further constraints, contours for the following measured mineral chemistry were plotted in grey: 1) garnet compositional contours for *z*(g) with measure range of 0.26–0.29; 2) omphacite compositional contours for *x*(o) with measured range 0.10–0.13; 3) omphacite compositional contours for *j(*o), measured range of 0.48–0.50 and (4) lowest abundance of kyanite in the peak field.

The peak conditions are more tightly constrained to 21–22 kbar and 670–690 °C, where the different isopleth ranges coincide in the peak field, as indicated by the orange star.

Figure 11. (a) Calculated *P–T* pseudosection for retrogressed eclogite, sample HOL13A_2015. The bulk composition at the top of the model is expressed as mol %. The white fields have a variance of two while the fields with darkest shade of blue have variance of seven. Mineral abbreviations used from Holland and Powell (1998).

*very were not labelled.The bold outline indicates peak mineral assemblage and yellow star designates approximate *P–T* conditions.

Contours were modelled as relative abundances (‘modes’) of the particular mineral. Abundances for phengite, omphacite, quartz, zoisite were overlain as grey regions. The peak conditions are more tightly constrained at 16–17 kbar and 680–700 °C where the isopleth ranges overlap in the peak field, indicated by the yellow star.

Figure 12. Figure comparing different elements in altered domains and their wall rocks. The chart represents the difference between the recrystallised pseudotachylite, peak eclogite and retrogressive and the granulite adjacent to them. Positive figures represent element 'gains' and negative values represent element 'loss' with respect to the wall rock. Original compositions for the wall-rock and altered rocks are provided in the supplementary data, Table S2.

Figure 13. Contour plot showing the difference in garnet abundance across *P–T* space for HOL7C*_2014 and HOL7C_2014 (Table 2). The field outlined by the dashed line represents the peak field in the model using the original, unmodified whole-rock composition. The solid line outlines the peak in the modified composition model and the star indicates the peak conditions modelled using the modified compositions. Red shades represent high differences in garnet abundance between the two models whereas blue shades represent lower differences in abundance.

Figure 14. (a) *P–T* path recorded by Holsnøy Island lithological domains is based on the calculated *P–T* pseudosections derived from sample HOL2A_2015 (Fig. 9), sample HOL7C_2014 (Fig. 10), sample HOL13A_2015 (Fig.11) The stars represent the approximate inferred peak metamorphic conditions for each of the 3 modelled stages. The figure also depicts different metamorphic textures occurring in the different stages of deformation. (b) Figure modified from Glodny *et al*. (2008) depicting the metamorphic evolution of the Holsnøy system. Circles represent extent of their calculated ages.

Figure 15. Figure showing (a) decrease in garnet abundance from granulite (white domain) to eclogite (green domain); (b) Plot constructed using TCInvestigator showing the variation of garnet abundance throughout *P–T* space for sample HOL7C_2014.

Table 1. Bulk-rock composition of chosen samples for phase modelling expressed in wt %.
*HOL4C_2014 was not modelled as it is only partially modified.

Table 2. Un-normalised bulk-rock composition in the system NCKFMASHTO expressed in mol % as input to THERMOCALC.
HOL7C* designates the original bulk composition for this sample (including relict garnet inherited from the granulitic protolith) whereas HOL7C is the modified bulk composition derived from removing the relict granulitic garnet from the whole-rock composition. The composition of the relict garnet is on the basis of electron micrprobe-measured mineral composition data (see Table 3).

$FeO^* = FeO_{(original)} + 2\times O$ as 'O' specifies the amount of excess oxygen required to oxidise FeO to create Fe_2O_3.

Table 3. Representative electron microprobe data of peak minerals in the three samples used for phase equilibria modelling: HOL2A_2015, HOL7C_2014 and HOL13A_2015.

Table 4. Representative mineral chemistry for samples use in forward phase equilibria modelling: HOL2A_2015, HOL7C_2014 and HOL13A_2015.

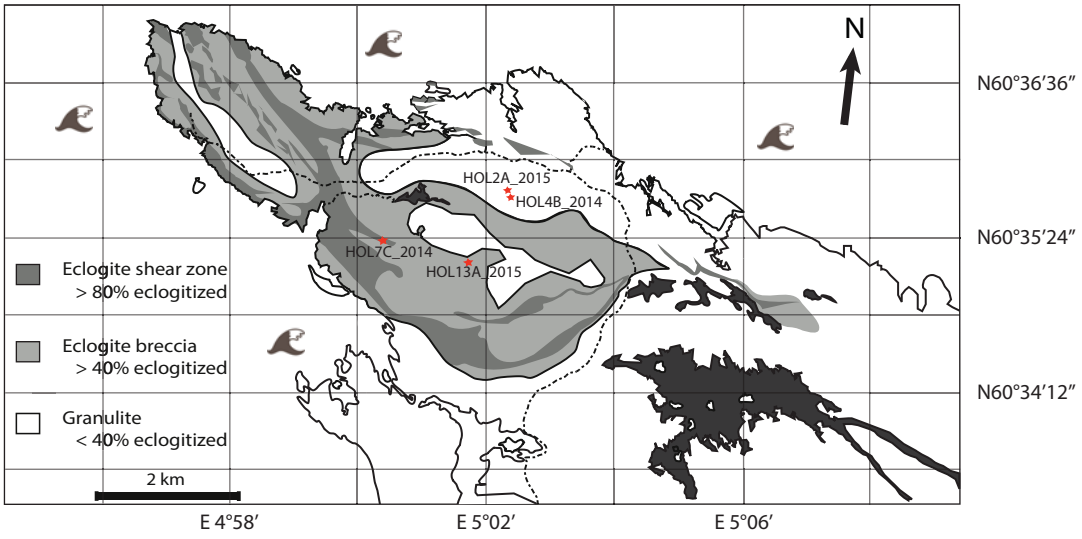
N
N60°36′36″
N60°35′24″
N60°34′12″
HOL2A_2015
HOL4B_2014
HOL7C_2014
HOL13A_2015
Eclogite shear zone
> 80% eclogitized
Eclogite breccia
> 40% eclogitized
Granulite
< 40% eclogitized
2 km
E 4°58′
E 5°02′
E 5°06′

Fig. 1

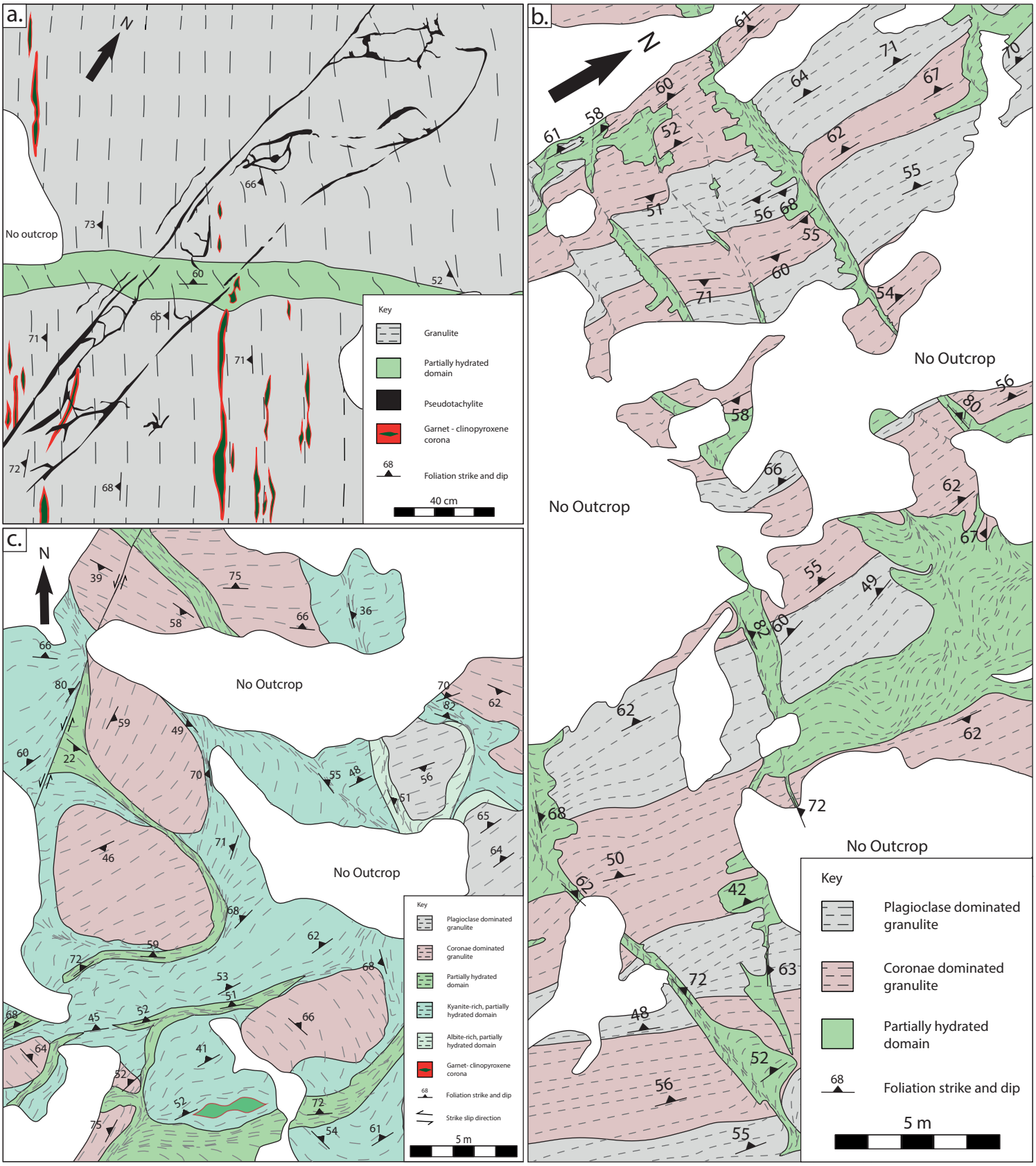
a.
N
No outcrop
Key
Granulite
Partially hydrated domain
Pseudotachylite
Garnet - clinopyroxene corona
Foliation strike and dip
40 cm
b.
N
No Outcrop
No Outcrop
No Outcrop
Key
Plagioclase dominated granulite
Coronae dominated granulite
Partially hydrated domain
Foliation strike and dip
5 m
c.
N
No Outcrop
No Outcrop
Key
Plagioclase dominated granulite
Coronae dominated granulite
Partially hydrated domain
Kyanite-rich, partially hydrated domain
Albite-rich, partially hydrated domain
Garnet- clinopyroxene corona
Foliation strike and dip
Strike slip direction
5 m

Fig. 2

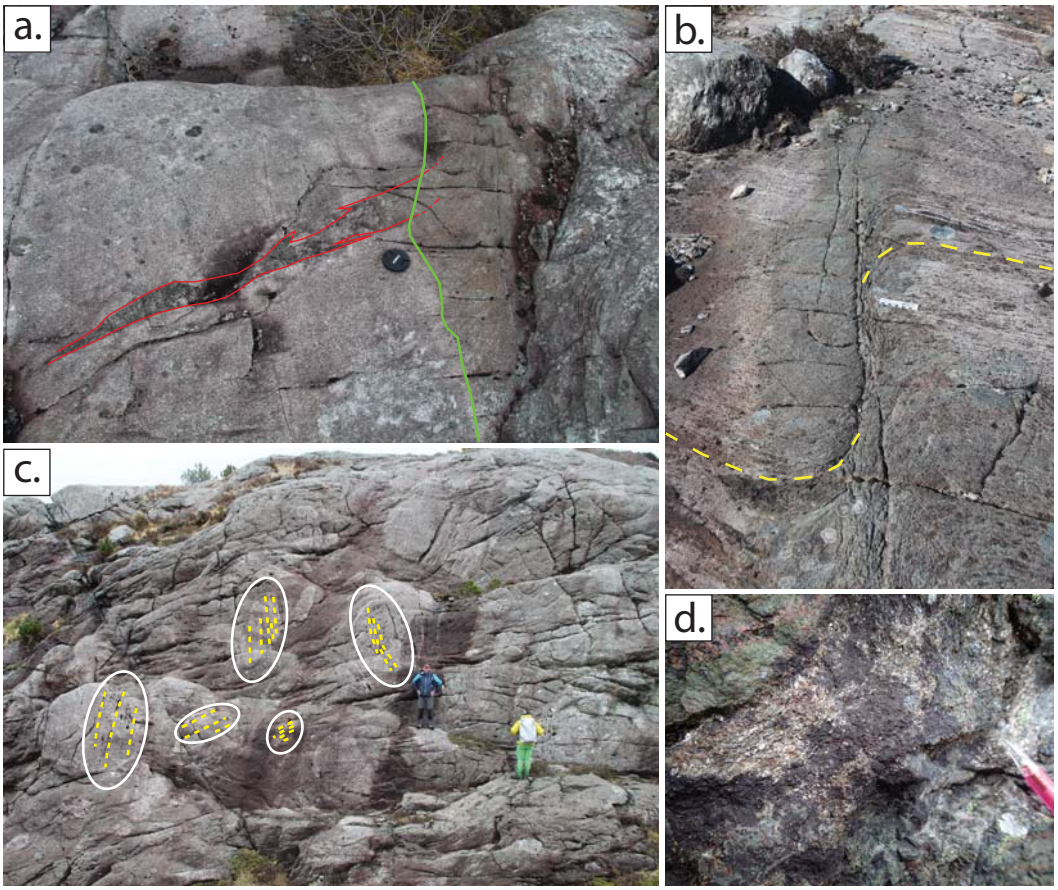

Fig. 3

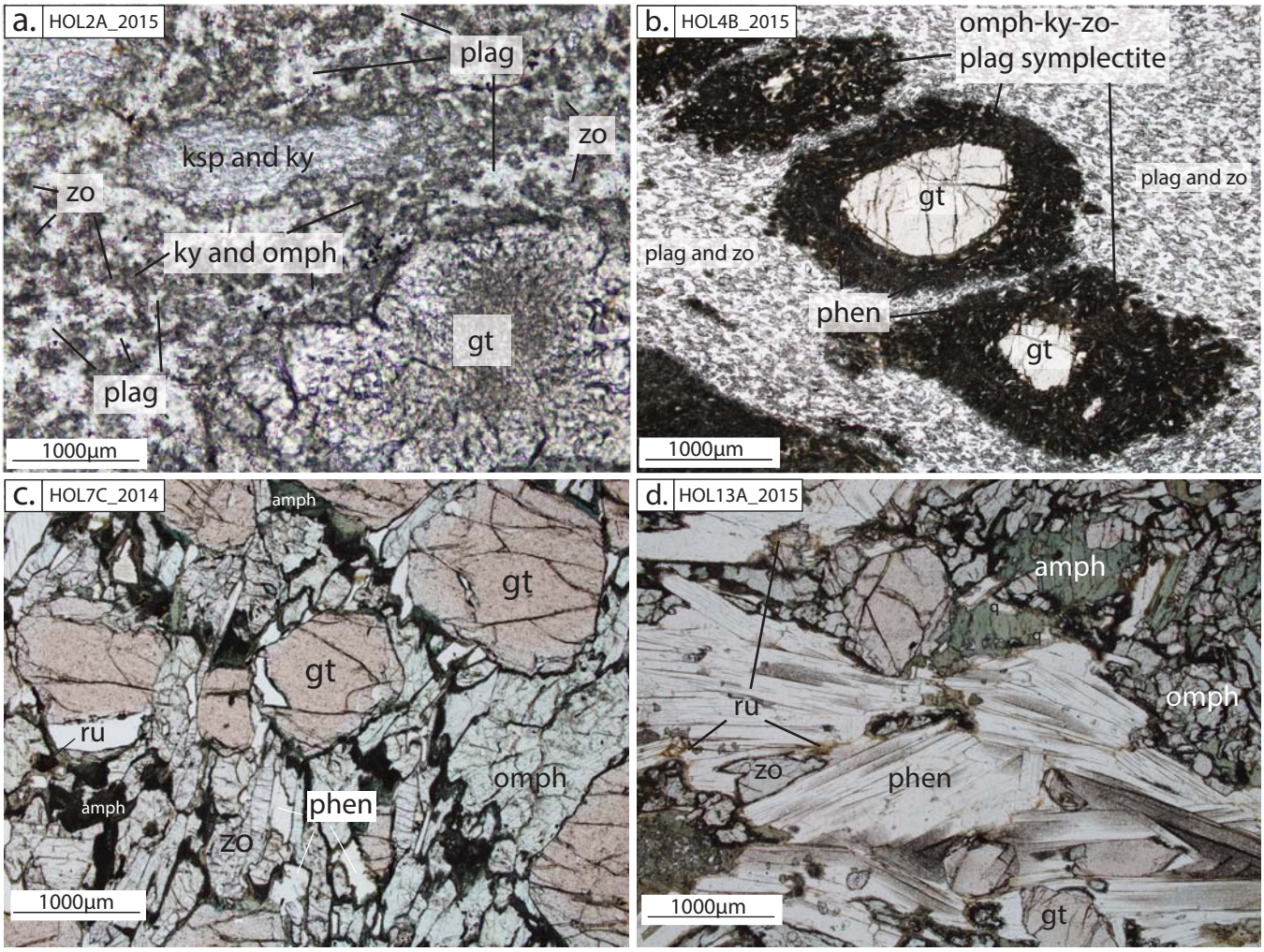
a.
HOL2A_2015
plag
zo
ksp and ky
zo
ky and omph
gt
plag
1000µm
b.
HOL4B_2015
omph-ky-zo-
plag symplectite
plag and zo
gt
plag and zo
phen
gt
1000µm
c.
HOL7C_2014
amph
gt
gt
ru
omph
amph
phen
zo
1000µm
d.
HOL13A_2015
amph
q
q
omph
ru
zo
phen
1000µm
gt

Fig. 4

HOL2A_2015 (stage 1)

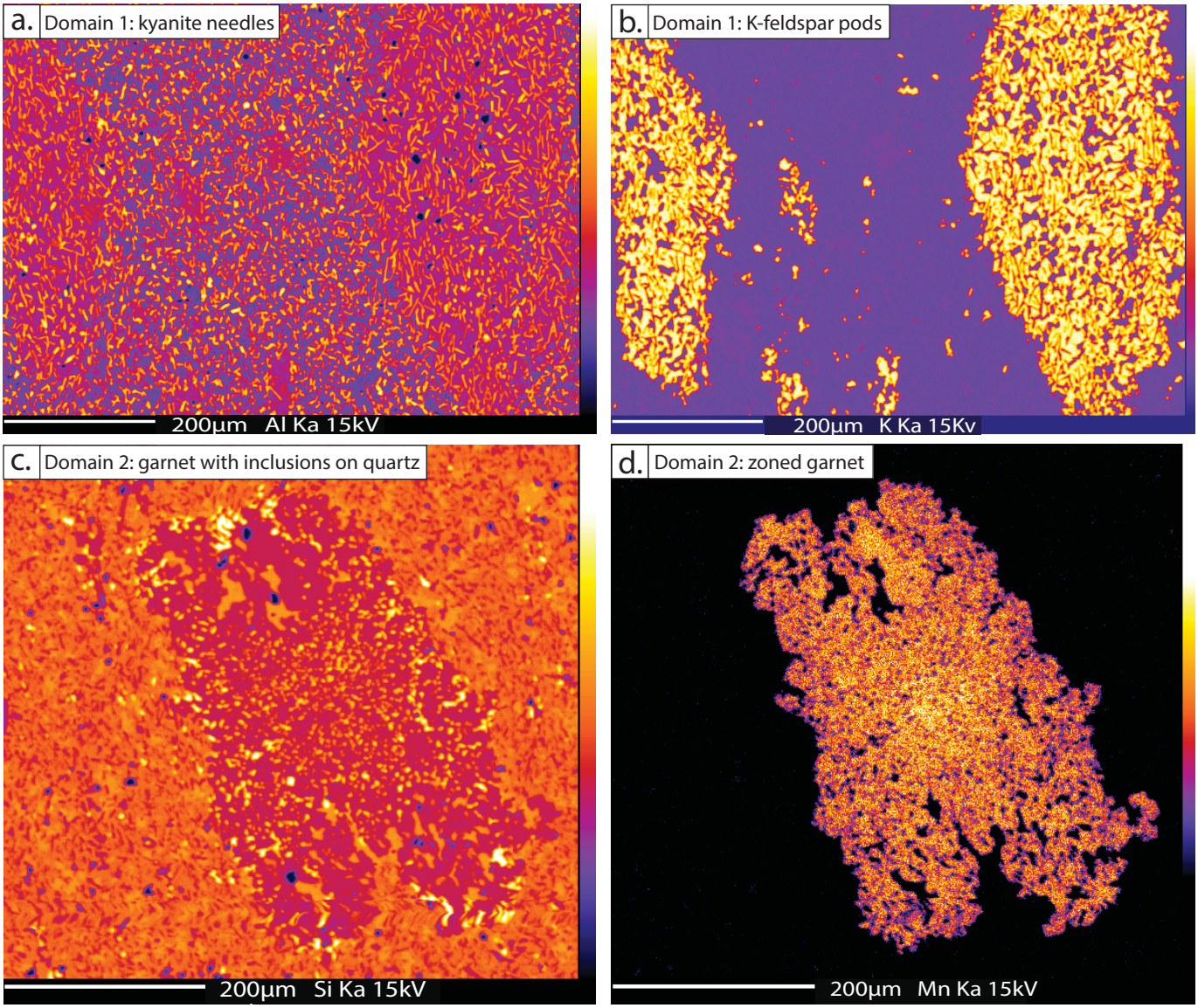

Fig. 5

HOL4B_2014 (stage 2)

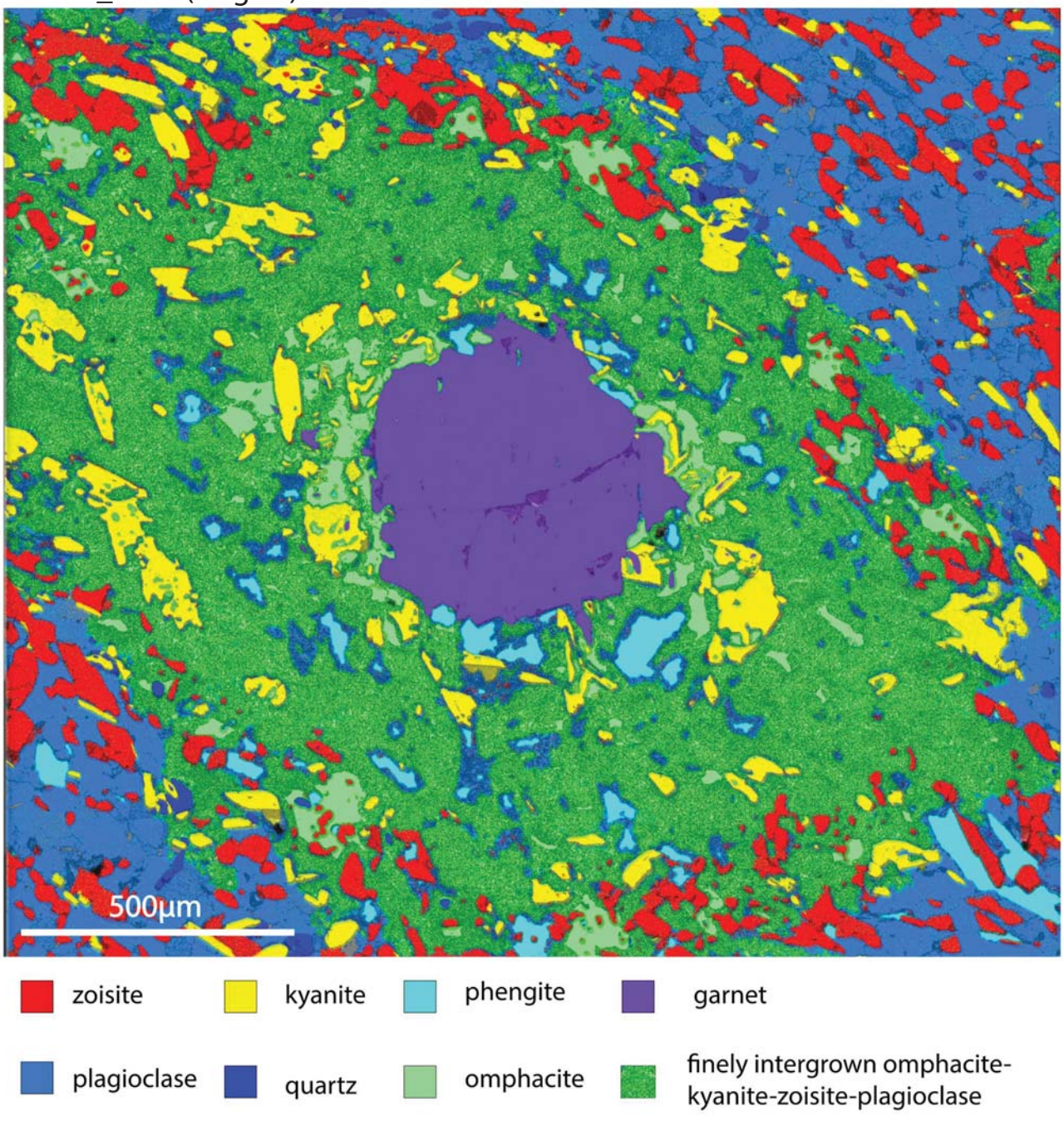

Fig. 6

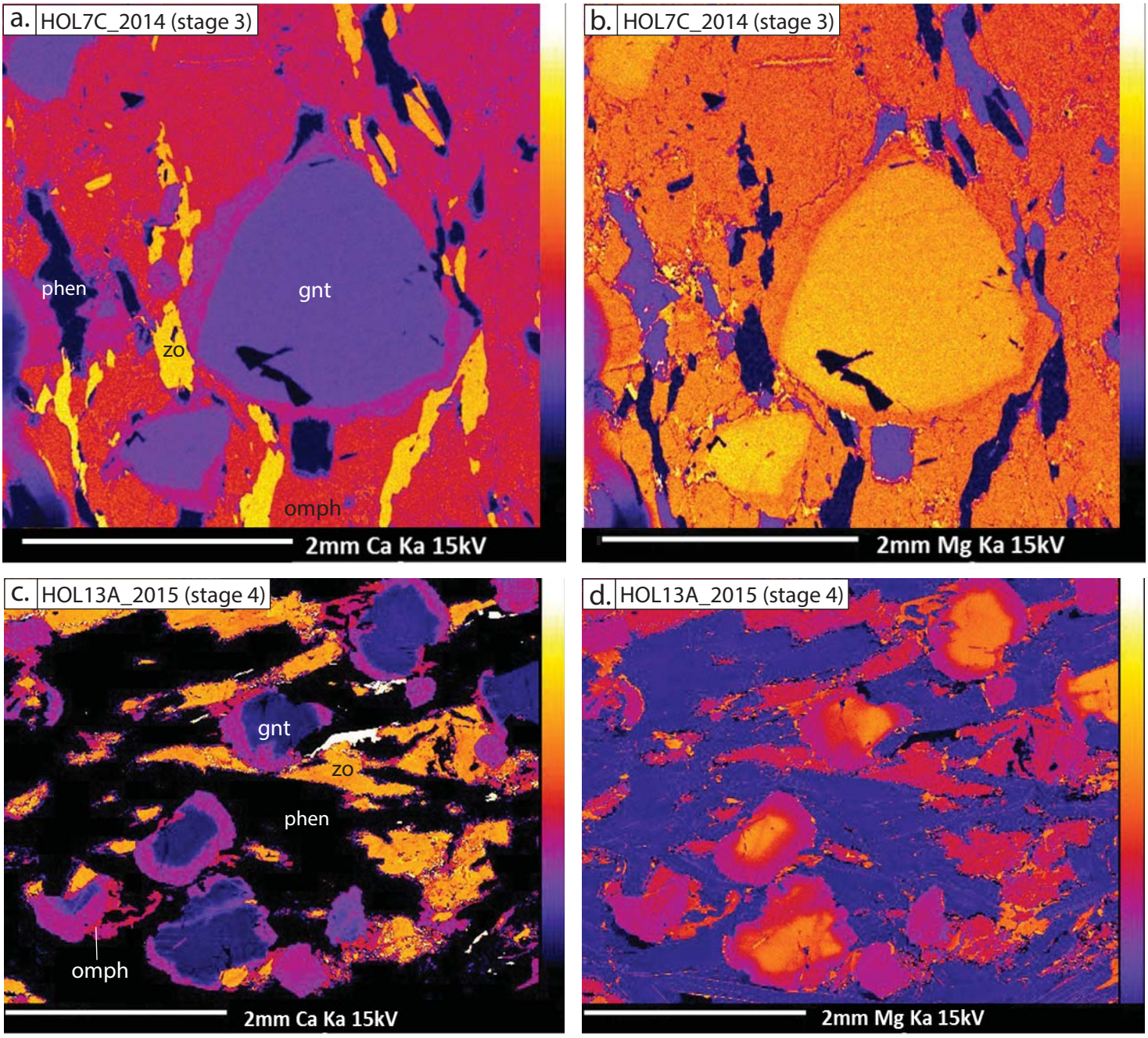
a. HOL7C_2014 (stage 3)
phen
gnt
zo
omph
2mm Ca Ka 15kV
b. HOL7C_2014 (stage 3)
2mm Mg Ka 15kV
c. HOL13A_2015 (stage 4)
gnt
zo
phen
omph
2mm Ca Ka 15kV
d. HOL13A_2015 (stage 4)
2mm Mg Ka 15kV

Fig. 7

Fig. 8

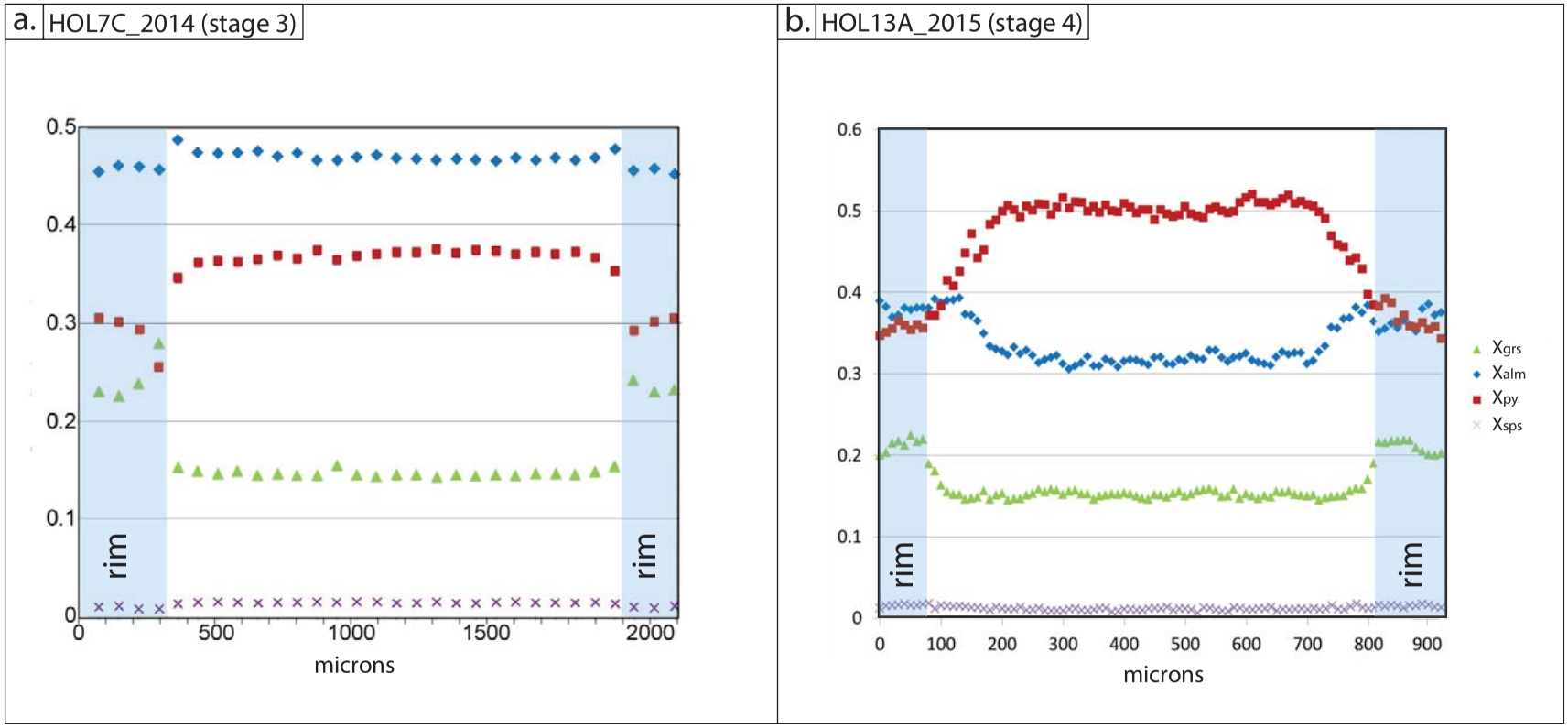
a.
HOL7C_2014 (stage 3)
0.5
0.4
0.3
0.2
0.1
0
rim
rim
0
500
1000
1500
2000
microns
b.
HOL13A_2015 (stage 4)
0.6
0.5
0.4
0.3
0.2
0.1
0
rim
rim
0
100
200
300
400
500
600
700
800
900
microns
Xgrs
Xalm
Xpy
Xsps

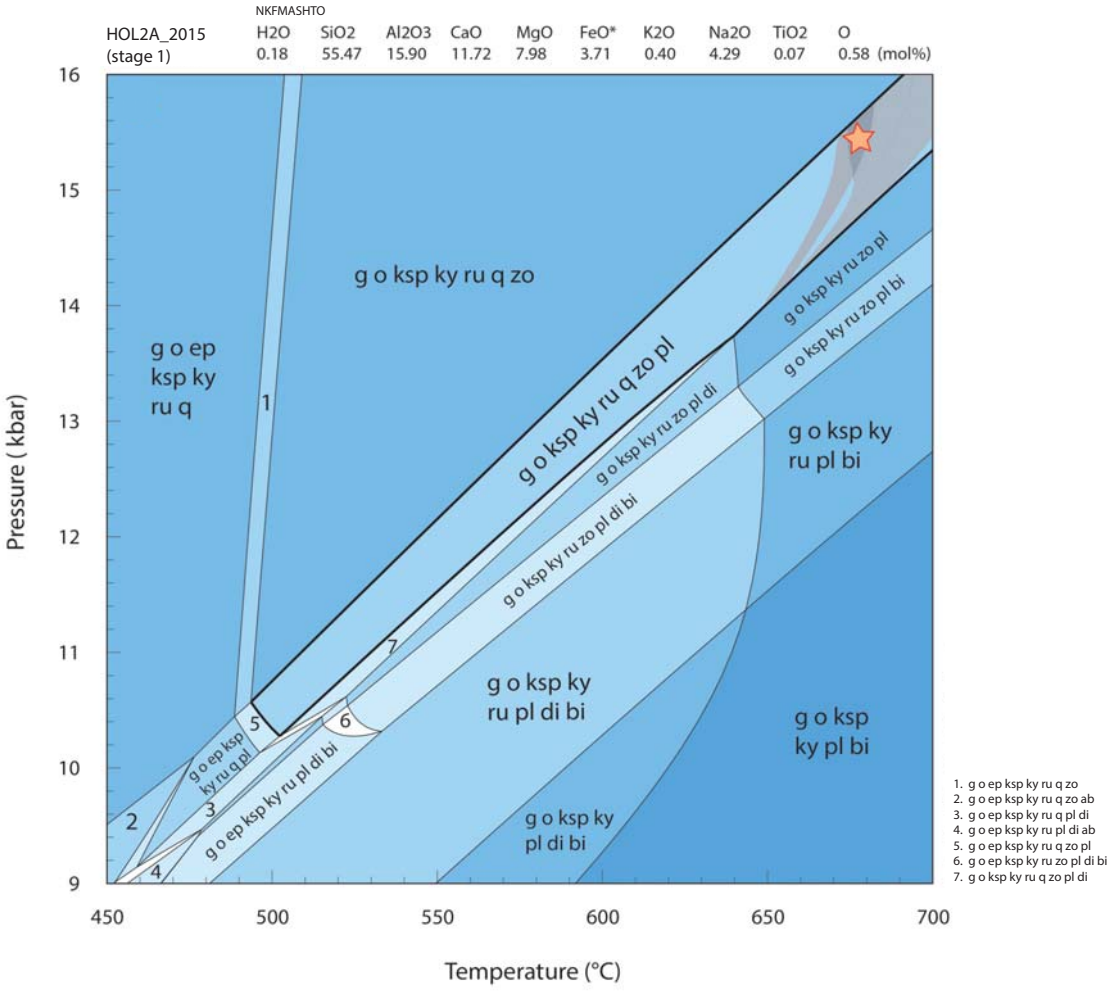
NKFMASHTO
HOL2A_2015
(stage 1)
H2O SiO2 Al2O3 CaO MgO FeO* K2O Na2O TiO2 O
0.18 55.47 15.90 11.72 7.98 3.71 0.40 4.29 0.07 0.58 (mol%)
Pressure (kbar)
Temperature (°C)
g o ep ksp ky ru q
g o ksp ky ru q zo
g o ksp ky ru q zo pl
g o ksp ky ru zo pl
g o ksp ky ru zo pl bi
g o ksp ky ru zo pl di
g o ksp ky ru pl bi
g o ksp ky ru pl di bi
g o ksp ky pl bi
g o ksp ky pl di bi
g o ep ksp ky ru q pl
g o ep ksp ky ru pl di bi
1. g o ep ksp ky ru q zo
2. g o ep ksp ky ru q zo ab
3. g o ep ksp ky ru q pl di
4. g o ep ksp ky ru pl di ab
5. g o ep ksp ky ru q zo pl
6. g o ep ksp ky ru zo pl di bi
7. g o ksp ky ru q zo pl di

Fig. 9

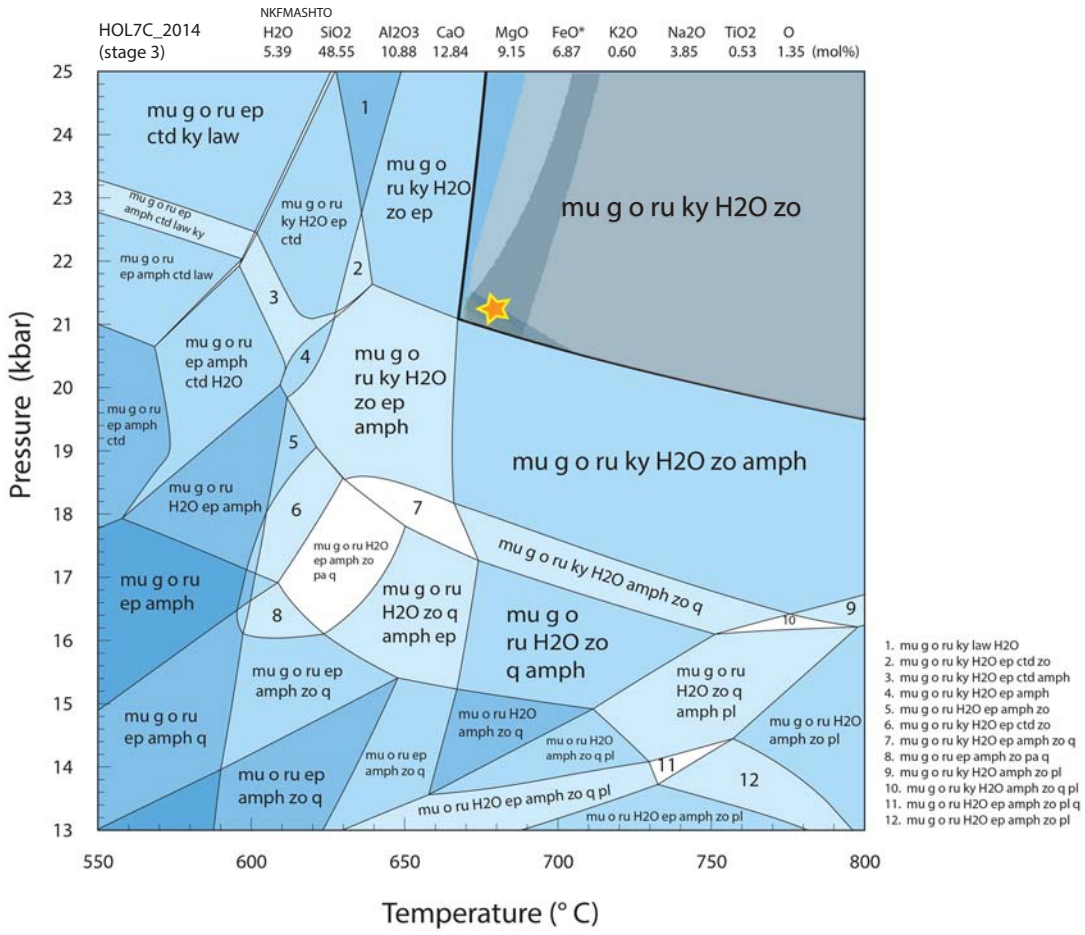
NKFMASHTO
HOL7C_2014
(stage 3)
H2O SiO2 Al2O3 CaO MgO FeO* K2O Na2O TiO2 O
5.39 48.55 10.88 12.84 9.15 6.87 0.60 3.85 0.53 1.35 (mol%)
mu g o ru ep ctd ky law
mu g o ru ky H2O zo ep
mu g o ru ky H2O zo
mu g o ru ep amph ctd law ky
mu g o ru ky H2O ep ctd
mu g o ru ep amph ctd law
mu g o ru ep amph ctd H2O
mu g o ru ky H2O zo ep amph
mu g o ru ep amph ctd
mu g o ru ky H2O zo amph
mu g o ru H2O ep amph
mu g o ru H2O ep amph zo pa q
mu g o ru ky H2O amph zo q
mu g o ru ep amph
mu g o ru H2O zo q amph ep
mu g o ru H2O zo q amph
mu g o ru ep amph zo q
mu g o ru H2O zo q amph pl
mu g o ru ep amph q
mu g o ru H2O amph zo q
mu g o ru H2O amph zo pl
mu o ru H2O amph zo q pl
mu o ru ep amph zo q
mu o ru ep amph zo q
mu o ru H2O ep amph zo q pl
mu o ru H2O ep amph zo pl
1 2 3 4 5 6 7 8 9 10 11 12
1. mu g o ru ky law H2O
2. mu g o ru ky H2O ep ctd zo
3. mu g o ru ky H2O ep ctd amph
4. mu g o ru ky H2O ep amph
5. mu g o ru H2O ep amph zo
6. mu g o ru ky H2O ep ctd zo
7. mu g o ru ky H2O ep amph zo q
8. mu g o ru ep amph zo pa q
9. mu g o ru ky H2O amph zo pl
10. mu g o ru ky H2O amph zo q pl
11. mu g o ru H2O ep amph zo pl q
12. mu g o ru H2O ep amph zo pl
Pressure (kbar)
25 24 23 22 21 20 19 18 17 16 15 14 13
550 600 650 700 750 800
Temperature (° C)

Fig. 10

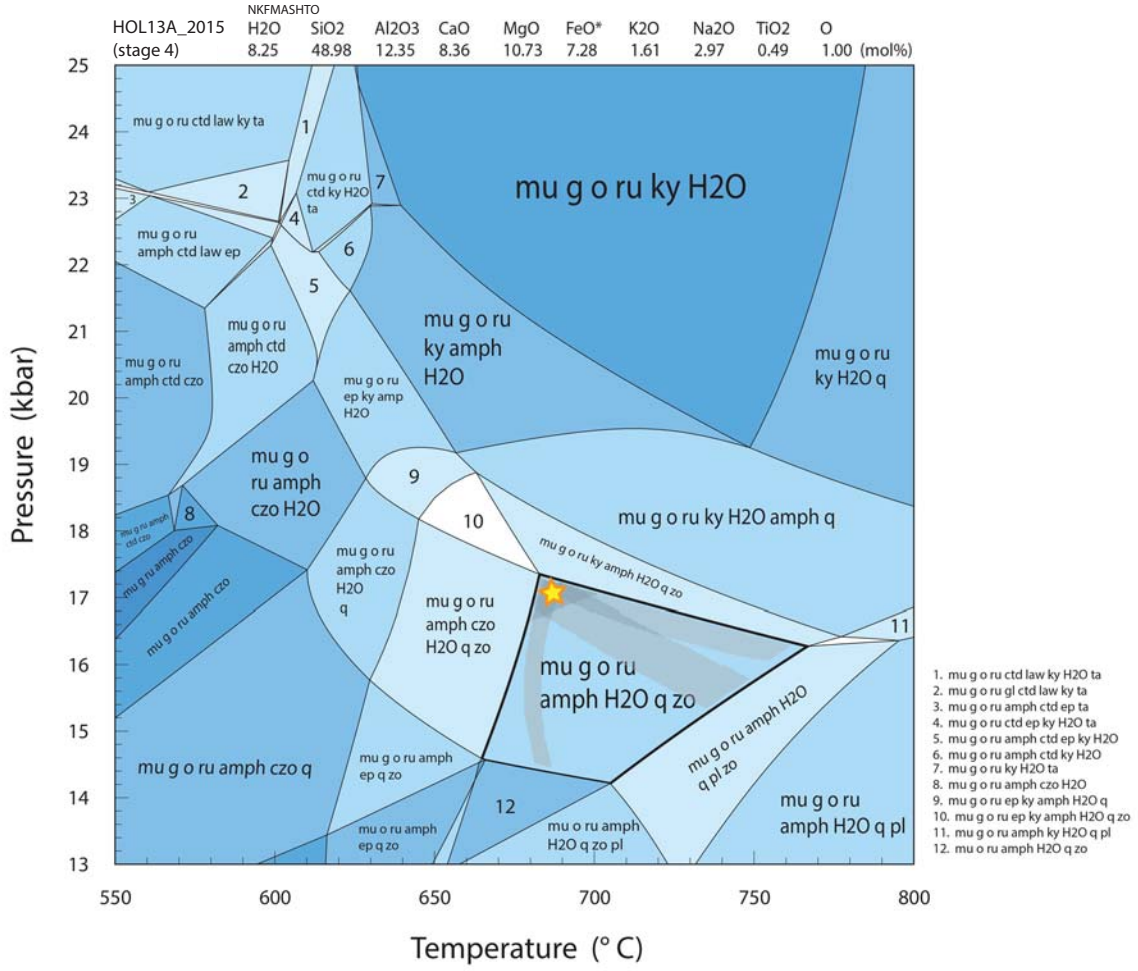
NKFMASHTO
HOL13A_2015
(stage 4)
H2O 8.25
SiO2 48.98
Al2O3 12.35
CaO 8.36
MgO 10.73
FeO* 7.28
K2O 1.61
Na2O 2.97
TiO2 0.49
O 1.00 (mol%)
Pressure (kbar)
Temperature (° C)
mu g o ru ctd law ky ta
mu g o ru ky H2O
mu g o ru amph ctd law ep
mu g o ru amph ctd czo H2O
mu g o ru ky amph H2O
mu g o ru ky H2O q
mu g o ru amph ctd czo
mu g o ru ep ky amp H2O
mu g o ru amph czo H2O
mu g o ru ky H2O amph q
mu g o ru amph czo H2O q
mu g o ru amph czo H2O q zo
mu g o ru ky amph H2O q zo
mu g o ru amph H2O q zo
mu g o ru amph czo q
mu g o ru amph ep q zo
mu o ru amph ep q zo
mu o ru amph H2O q zo pl
mu g o ru amph H2O q pl zo
mu g o ru amph H2O q pl
1. mu g o ru ctd law ky H2O ta
2. mu g o ru gl ctd law ky ta
3. mu g o ru amph ctd ep ta
4. mu g o ru ctd ep ky H2O ta
5. mu g o ru amph ctd ep ky H2O
6. mu g o ru amph ctd ky H2O
7. mu g o ru ky H2O ta
8. mu g o ru amph czo H2O
9. mu g o ru ep ky amph H2O q
10. mu g o ru ep ky amph H2O q zo
11. mu g o ru amph ky H2O q pl
12. mu o ru amph H2O q zo

Fig. 11

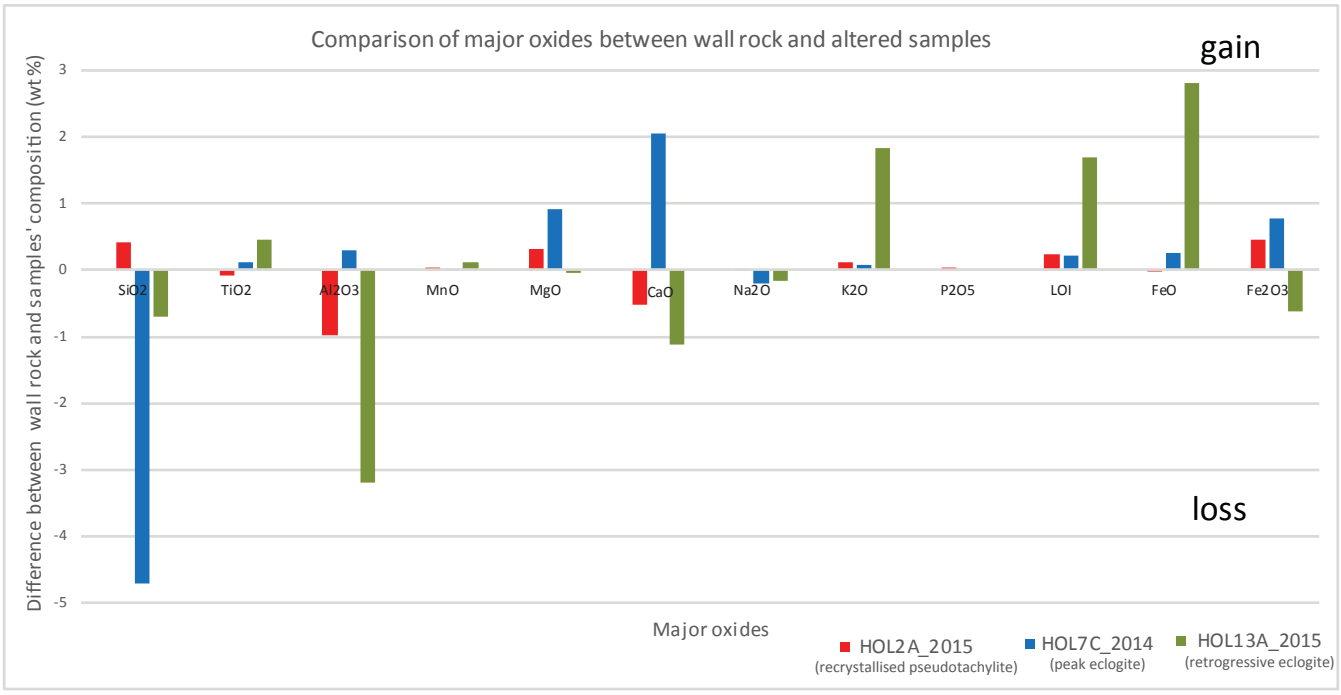
Comparison of major oxides between wall rock and altered samples
gain
loss
Difference between wall rock and samples' composition (wt %)
3
2
1
0
-1
-2
-3
-4
-5
SiO2
TiO2
Al2O3
MnO
MgO
CaO
Na2O
K2O
P2O5
LOI
FeO
Fe2O3
Major oxides
HOL2A_2015
(recrystallised pseudotachylite)
HOL7C_2014
(peak eclogite)
HOL13A_2015
(retrogressive eclogite)

Fig. 12

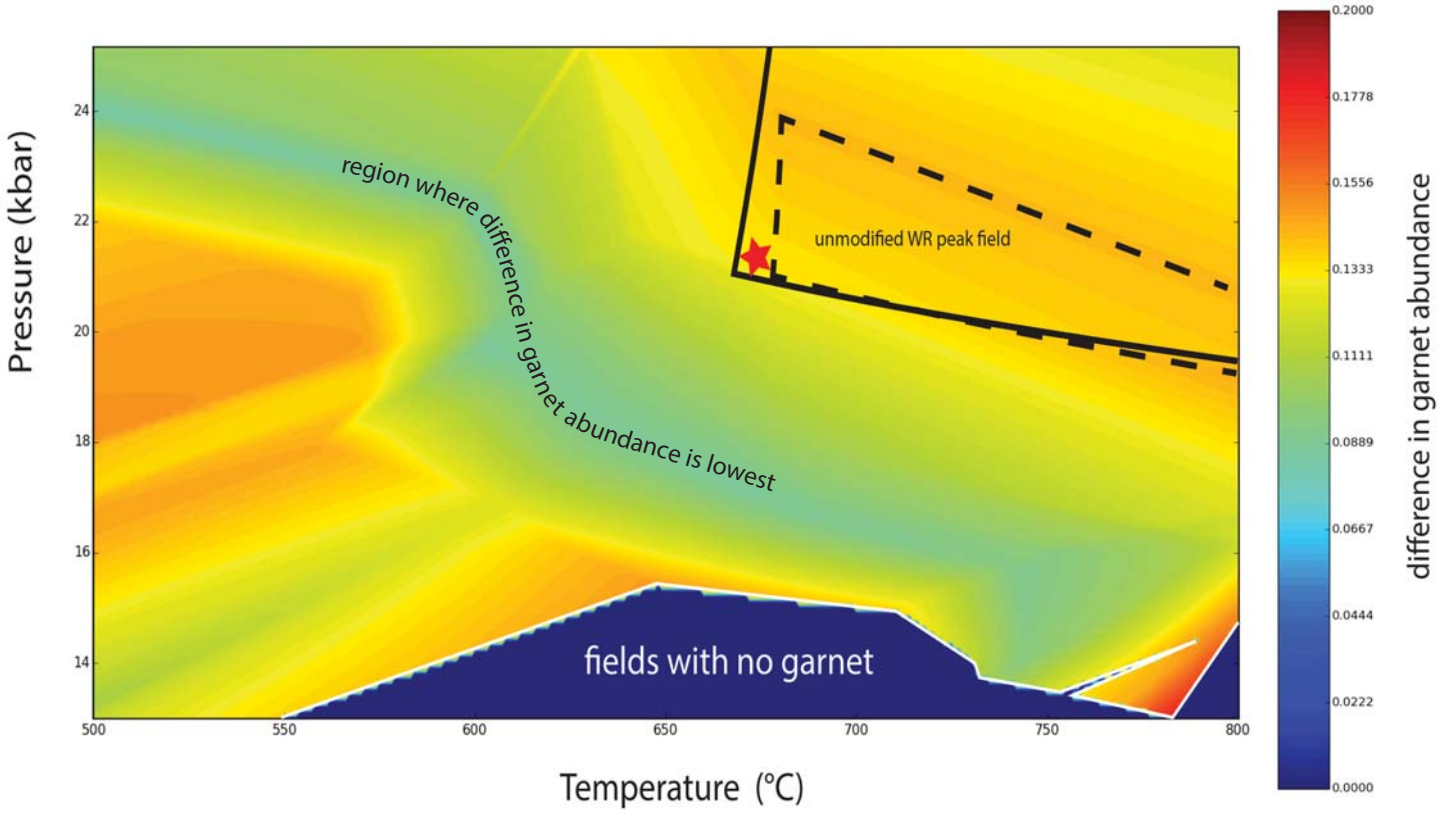
Pressure (kbar)
24
22
20
18
16
14
region where difference in garnet abundance is lowest
unmodified WR peak field
fields with no garnet
500
550
600
650
700
750
800
Temperature (°C)
0.2000
0.1778
0.1556
0.1333
0.1111
0.0889
0.0667
0.0444
0.0222
0.0000
difference in garnet abundance

Fig. 13

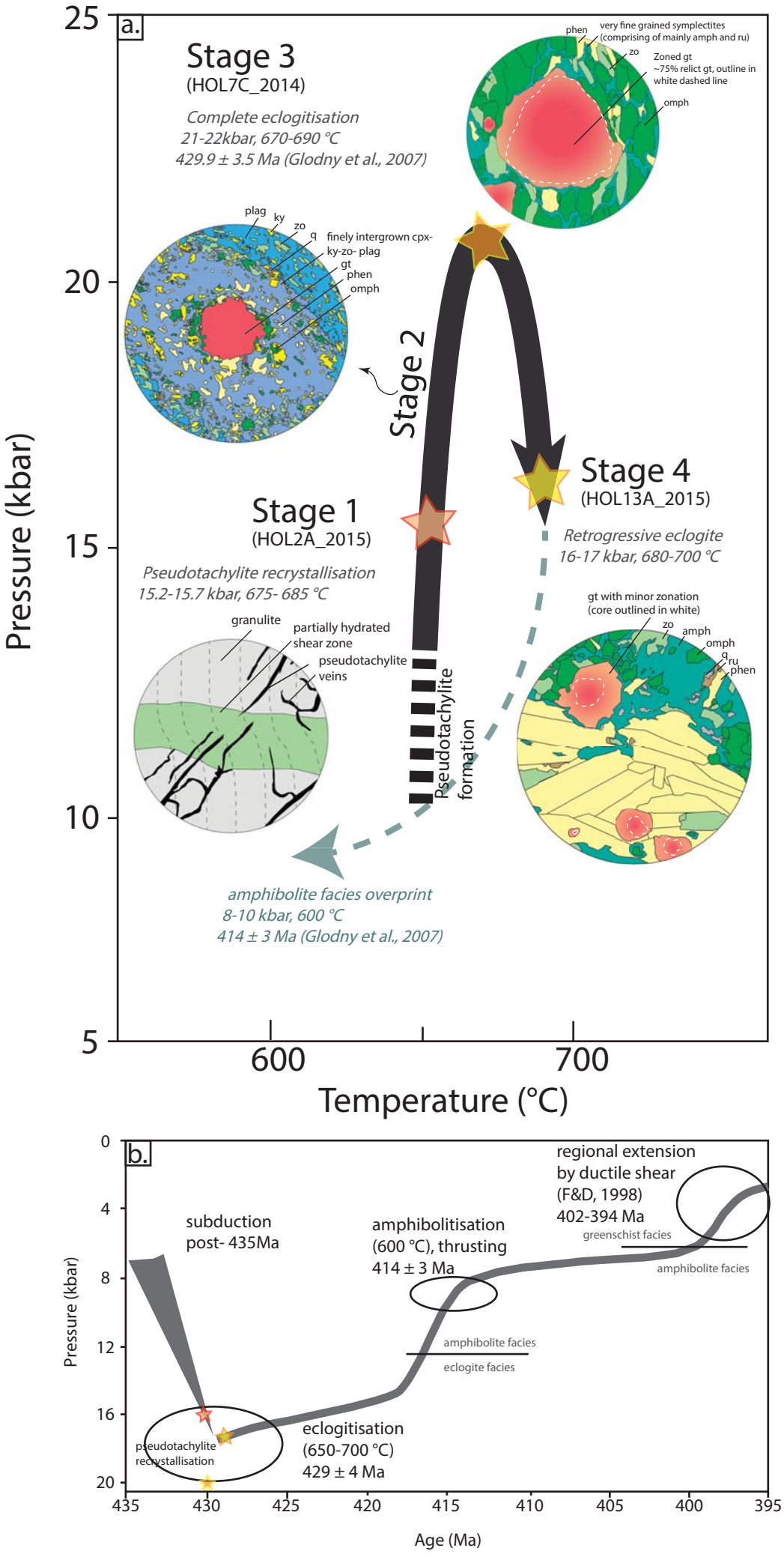
a.
Stage 3
(HOL7C_2014)
Complete eclogitisation
21-22kbar, 670-690 °C
429.9 ± 3.5 Ma (Glodny et al., 2007)
phen
very fine grained symplectites
(comprising of mainly amph and ru)
zo
Zoned gt
~75% relict gt, outline in
white dashed line
omph
plag
ky
zo
q
finely intergrown cpx-
ky-zo- plag
gt
phen
omph
Stage 2
Stage 4
(HOL13A_2015)
Retrogressive eclogite
16-17 kbar, 680-700 °C
Stage 1
(HOL2A_2015)
Pseudotachylite recrystallisation
15.2-15.7 kbar, 675- 685 °C
granulite
partially hydrated
shear zone
pseudotachylite
veins
Pseudotachylite
formation
gt with minor zonation
(core outlined in white)
zo
amph
omph
q
ru
phen
amphibolite facies overprint
8-10 kbar, 600 °C
414 ± 3 Ma (Glodny et al., 2007)
Pressure (kbar)
25
20
15
10
5
600
700
Temperature (°C)
b.
regional extension
by ductile shear
(F&D, 1998)
402-394 Ma
greenschist facies
amphibolite facies
subduction
post- 435Ma
amphibolitisation
(600 °C), thrusting
414 ± 3 Ma
amphibolite facies
eclogite facies
eclogitisation
(650-700 °C)
429 ± 4 Ma
pseudotachylite
recrystallisation
Pressure (kbar)
0
4
8
12
16
20
435
430
425
420
415
410
405
400
395
Age (Ma)

Fig. 14

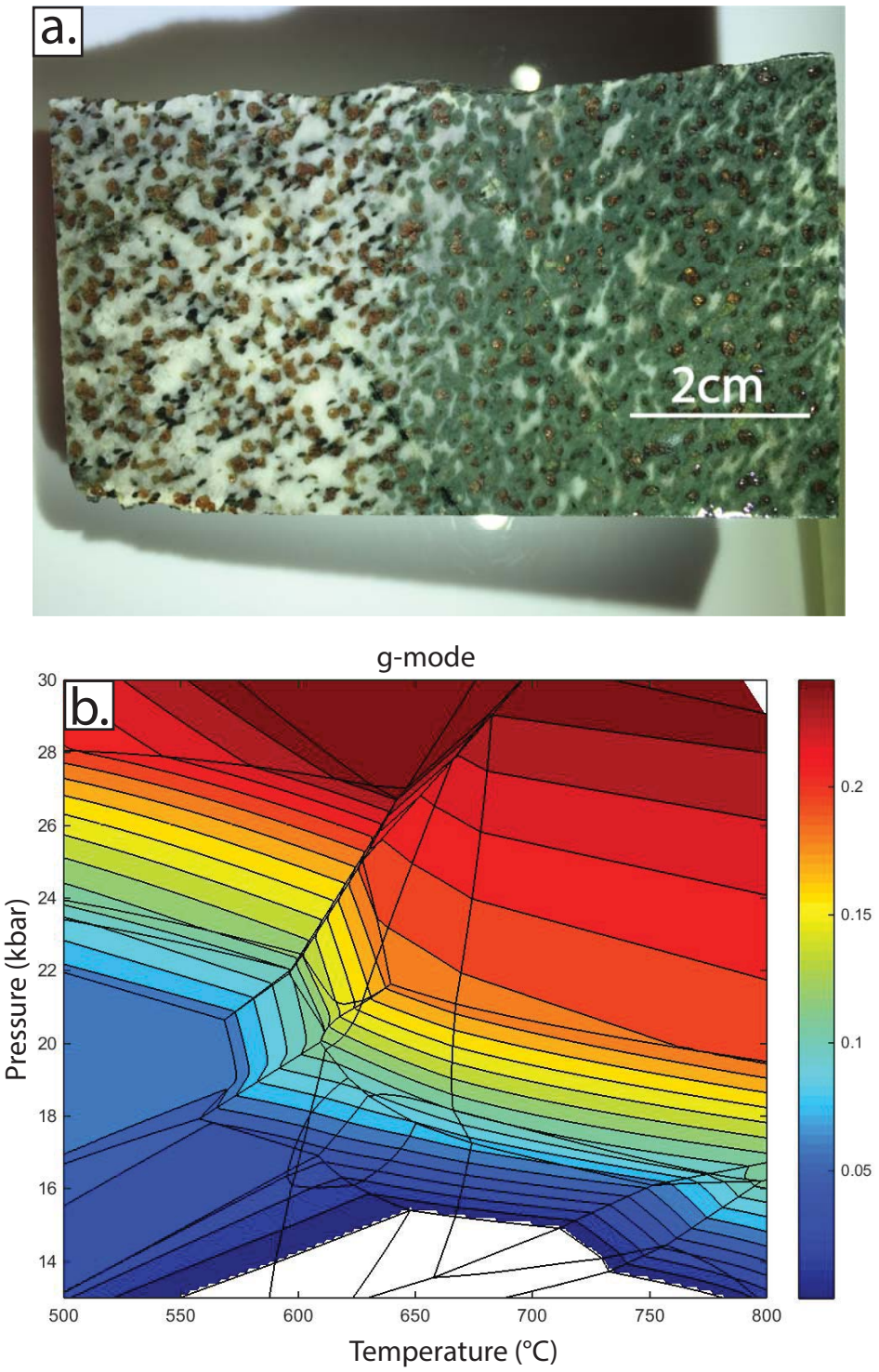
a.
2cm
g-mode
b.
Pressure (kbar)
Temperature (°C)
30
28
26
24
22
20
18
16
14
500
550
600
650
700
750
800
0.2
0.15
0.1
0.05

Fig. 15